

PREPARATION AND CHARACTERIZATION OF  
POLYETHYLENE-OXIDE (PEO) SOLUTION

By

MARCUS LANDER

Bachelor of Science in Mechanical Engineering and

Aerospace Engineering

Oklahoma State University

Stillwater, OK

2015

Submitted to the Faculty of the  
Graduate College of the  
Oklahoma State University  
in partial fulfillment of  
the requirements for  
the Degree of  
MASTER OF SCIENCE  
May, 2018

PREPARATION AND CHARACTERIZATION OF  
POLYETHYLENE-OXIDE (PEO) SOLUTION

Thesis Approved:

Dr. Brian R. Elbing

---

Thesis Adviser

Dr. Jamey Jacob

---

Dr. Arvind Santhanakrishnan

---

## ACKNOWLEDGEMENTS

This material is based upon work supported by the National Science Foundation under Grant No. 1604978 (Dr. Ronald Joslin, Program Manager).

I would like to thank Dr. Elbing for his guidance and mentorship on this project.

I would also like to thank JW Wallace and John Franke for their assistance and hard work in this research project. They showed a dedication to this far beyond what I would have expected of anyone.

Next, I would like to thank my friend Haylie “Reese” Hadzeriga for their artistic depiction of the mixing process used when diluting polymers in the pressure vessel. It was not something I could easily depict on my own.

Lastly, but certainly not the least, I’d like to thank my friend Paul Sanders, an electrical engineer, who helped me with the circuits and calibration of the function generator. Furthermore, he helped me in identifying the mysterious bug in the Raspberry Pi that ultimately led to us abandoning the Pi in favor of the function generator.

Name: MARCUS LANDER

Date of Degree: MAY, 2018

Title of Study: PREPARATION AND CHARACTERIZATION OF POLYETHYLENE-  
OXIDE (PEO) SOLUTION

Major Field: MECHANICAL AND AEROSPACE ENGINEERING

Abstract: For years, it has been known that the addition of a small amounts of polymers, or other materials, to water or other liquids can help reduce the skin friction of a general liquid when flowing past a solid surface, known as drag reduction. When mixing these materials with water, it is important that all samples are as consistent as possible. The current work seeks to identify a robust method of preparation that results in consistent and accurate batches of polymer solution at a desired concentration. A set of preparation procedures is described, and characterization of these batches will be based upon molecular weight, viscosity, and other polymer parameters. The molecular weight is characterized using a pressure drop apparatus, and viscosity is characterized using a rheometer. Additionally, this work will briefly focus on items of avoidance during preparation. The solutions prepared with the method described herein showed consistent measurements for molecular weight for concentrations of 10 ppm and 15 ppm. A batch with a concentration of 1000 ppm is shown to have a high repeatability during viscosity tests. Based on these results, the method of preparation described successfully produces polymer solutions with consistent characteristics at a desired concentration.

## TABLE OF CONTENTS

I. INTRODUCTION.....	1
II. POLYMER PREPARATION.....	4
2.1 Polymer Type.....	4
2.2 Preparation Process .....	5
2.3 Limitations and Recommendations for Preparation Method.....	7
III. POLYMER CHARACTERIZATION.....	10
3.1 Molecular Weight.....	10
3.1.1 Measurement approach.....	10
3.1.2 Virk tube design .....	12
3.1.3 Test procedures.....	14
3.1.4 Data reduction .....	21
3.1.5 Data analysis and calculations.....	24
3.1.6 Uncertainty analysis .....	25
3.1.7 Results .....	39
3.2 Apparent viscosity.....	43
3.2.1 Rheometer .....	43
3.2.2 Test procedures.....	43
3.2.3 Data analysis and model fitting.....	44
3.2.4 Uncertainty analysis .....	46
3.3 Relaxation time .....	47
3.3.1 Intrinsic viscosity.....	47
3.3.2 Zimm time .....	48
3.3.3 Kalashnikov time.....	49
3.3.4 Results .....	49
3.4 Polymer parameter calculations .....	50
3.4.1 Weissenberg number .....	50
3.4.2 Viscosity ratio ( $\mu^*$ ).....	51
3.4.3 Length ratio .....	51
IV. CASE STUDY: SYRINGE PUMP DEGRADATION .....	53
4.1 Syringe pump description.....	53
4.2 Experimental procedure .....	57
4.3 Results.....	58
V. SUMMARY AND CONCLUSIONS.....	61
REFERENCES .....	62

APPENDIX A: DETAILED POLYMER PREPARATION PROCEDURES .....	68
APPENDIX B: ANALYSIS CODE .....	72
APPENDIX C: EXTENDED UNCERTAINTY ANALYSIS DATA .....	82
APPENDIX D: NOMENCLATURE.....	85

## LIST OF TABLES

Table 1: Example data table for recording data during experimentation.....	20
Table 2: Cole-Parmer digital scale uncertainty measurement data.....	27
Table 3: Cole-Parmer Uncertainty Measurement Data, Beaker Data.....	29
Table 4: CPWplus-35 Uncertainty Measurement Data, Scale Measurement.....	29
Table 5: CPWplus-35 Uncertainty Measurement Data, Bucket Measurement.....	30
Table 6: Voltage Uncertainty Measurement Data.....	31
Table 7: General summary of molecular weight estimations. Error calculations are based on the estimated molecular weight of WSR-301 ( $M_w \cdot 10^6 = 4.0$ ) provided by the DOW Chemical Company.....	41
Table 8: Uncertainty estimations for Time, $\Delta x$ , mass measurement of the CPWplus-35 scale, the Cole-Parmer scale, and temperature measurement.....	42
Table 9: Uncertainty estimations for $V_0$ , $V_{\text{measure}}$ , and $\Delta V$ .....	43
Table 10: Standard deviation data of viscosity datasets for 1, 12, and 18 hour samples.....	47
Table 11: Testing parameters for viscosity testing and resulting relaxation time values.....	49
Table 12: Calculated values and basic statistics of the mass flow rate calibration.....	57
Table 13: Molecular weight results for case study samples.....	58
Table 14: Extended uncertainty data for concentration 15 ppm.....	83
Table 15: Extended uncertainty data for concentration 10 ppm.....	84

## LIST OF FIGURES

Figure 1. A demonstration of how the molecular weight of a polymer solution degrades in the presence of metal. ....	9
Figure 2. Sketch of fully developed turbulent pipe flow, which is required to relate the pressure drop within the Virk tube with skin-friction. ....	12
Figure 3. Schematic of the Virk tube (pressure drop apparatus) used for characterization of the polymer batches. ....	13
Figure 4. (left) Wiring diagram for the PX2300 pressure transducer. The voltage across the monitoring load is what is recorded by the data acquisition system. (right) Graph of the minimum required supply voltage for a given loop resistance. If minimum voltage is not supplied the performance is unpredictable. Both illustrated are adapted from Omega Engineering (1999). ....	14
Figure 5: Illustration of how to use the swirling motion of the water to mix the polymer solution with water while diluting. Drawn by Haylie "Reese" Hadzeriga.....	17
Figure 6. Schematic of the pressure transducer (PX2300, Omega Engineering) illustrating the location of the bleed screws. This illustration is adapted from the PX2300 user manual (Omega Engineering, 1999).....	18
Figure 7: Raw voltage output of two test conditions during DAQ. There are two clear upper and lower regions of the signal data. The lower region ( $V_{zero}$ ) corresponds to the no-flow condition, and the upper region ( $V_{measure}$ ) is when there is a working fluid flowing through the Virk tube. When the signal changes from an upper region to a lower region, this is considered the end of that test condition.....	22
Figure 8: Zoomed in raw voltage output, demonstrating how a $V_{measure}$ signal cannot be analyzed entirely. After a certain amount of time the $V_{measure}$ has stabilized to its true value. ....	23
Figure 9: PK plot showing the relationship between the Fanning friction factor and the pipe diameter based Reynolds Number. Lines corresponding to laminar flow, turbulent Newtonian flow (PK law), and the empirically derived Maximum Drag Reduction (MDR) limit (Virk, 1975). ....	24
Figure 10: Simple sketch demonstrating the potential uncertainty introduced by a dip (warp) in the measuring tape used when measuring the length of the Virk tube measurement section. The tape measure would be measuring $2C$ while the actual length was $L$ .....	26
Figure 11: Brief comparison of Cole-Parmer scale data readout vs the target mass value. The dashed line represents the average values of the 3 trials.....	28
Figure 12: Voltage signal used in for the uncertainty analysis. ....	32
Figure 13: Representation of drag reduction uncertainty using error bars. Concentration 15 ppm. ....	38
Figure 14: Representation of drag reduction uncertainty using error bars. Concentration 10 ppm. ....	38

Figure 15: The above figure shows how the drag reduction profiles of the polymer solutions vary based on concentration.....	41
Figure 16: A Comparison of the viscous properties of WSR-301, concentration 1000 ppm, according to the time between preparation and testing.....	45
Figure 17: A zoomed in version of Figure 16.....	46
Figure 18: Weissenberg number vs shearing rate .....	50
Figure 19. Picture of the syringe pump designed and built by Bonk et al. (2017).....	54
Figure 20: New wiring setup for the syringe pump. The dashed red line represents this red/white wire, and the dashed green line represents the green/white wire. ....	55
Figure 21: Instantaneous mass measurements varying with frequency. ....	56
Figure 22: Mass flow rate calibrated against frequency, plotted with the change in standard deviation, which also varies with frequency. ....	57
Figure 23: Demonstration of degradation of polymer solution after being plunged through the syringe pump.....	59
Figure 24: VBA GUI Interface for the visual data analysis program. ....	73

## CHAPTER I

### INTRODUCTION

The use of dilute polymer solutions for drag reduction was originally observed in the late 1940s (Toms, 1948; Mysels, 1949), but the seminal work was produced in the late 1960s by Preetinder S. Virk (Virk et al., 1967; 1970; Virk, 1975), Jacques Zakin (Hershey & Zakin, 1967a,b; Patterson et al., 1969; Liaw et al., 1971; Zakin & Hunston, 1980), and their colleagues. They observed that it was possible to reduce the skin friction of a liquid turbulent flow by up to 75% with the addition of small amounts (~10 ppm) of polymer solution. This phenomenon is known as polymer drag reduction, and the possible applications have captured the attention of businesses, militaries, and more. While there have been recent efforts to implement polymer drag reduction in external flows (Truong, 2001; Elbing et al., 2011), all of the pioneering efforts focused on the use of dilute solutions of polymer in pipe flows (Virk, 1975). Pipe flows have the advantage of the pressure drop across a given length of pipe being directly related to the wall shear stress (i.e. skin-friction), which allows the drag reduction to be defined as the change in the pressure drop from standard conditions (Newtonian flow),  $\%DR = (1 - \Delta P_p / \Delta P_s) \times 100$ . Here  $\Delta P_s$  is the standard pressure drop experienced and  $\Delta P_p$  is the pressure drop in a flow with polymer drag reduction.

In addition to other issues, polymer drag reduction studies are complicated by issues with ensuring that the test samples are identical between test conditions. Some of the concerns are (though not limited to) sample degradation, proper mixing, and even consistency in sample behavior. While consistent preparation procedures and precise measurements can alleviate most of these issues, sample degradation is more difficult to prevent (and confirm whether or not degradation occurred).

Degradation is the breakdown of the polymer chains, which can happen for many reasons with sources being mechanical, chemical, and/or thermal. The polymer solution is essentially a homogeneous mixture of very long, linear polymer chains suspended in solution of water. The length of these chains is directly related to drag reduction efficiency of the solution (Virk 1975; Kalashnikov, 1998; Elbing et al., 2009; 2011). Hence, confirming the amount of degradation to a test sample is extremely important for polymer drag reduction studies. Since the polymer chains are linear, the length of the chains are directly related to their molecular weight, which suggests monitoring molecular weight is the ideal means of quantifying polymer degradation. Unfortunately, traditional means of measuring the molecular weight distribution of a polymer solution is not effective at these extremely high molecular weight solutions, especially high molecular weight polyethylene oxide.

Polyethylene oxide is an inexpensive, synthetic biodegradable polymer that has seen a wide adoption in industry, and it comes in a wide variety of molecular weights to suit many applications (Truong, 2001). It has also been a primary focus of many recent polymer drag reduction studies (Wei & Willmarth, 1992; Fontaine et al., 1992; White et al., 2004; Petrie et al., 2005; Hou et al., 2008; Winkel et al., 2009; Elbing et al., 2009, 2010a,b, 2011, 2013; Shetty & Solomon, 2009; Somandepalli et al., 2010; Zadrazil et al., 2012) because it is extremely efficient (75% drag reduction with ~10 ppm), which is required if polymer drag reduction is to be implemented on external flows. The current work focuses on robust means of preparing and

characterizing polyethylene oxide for turbulent boundary layer studies. A method for preparation has been proposed herein that attempts to create batches of polymer solution with consistent properties at any desired concentration. To demonstrate the consistency of the batches, the solutions are characterized in terms of their mean molecular weight via a technique pioneered by Vanapalli et al. (2006, 2006) and Elbing et al. (2009, 2011) as well as their apparent viscosity and relaxation time. The error associated with these characterization processes are also examined in detail to better quantify the accuracy of the results.

## CHAPTER II

### POLYMER PREPARATION

#### **2.1 Polymer Type**

The polymer used in this study is polyethylene oxide (PEO), specifically WSR-301 (Dow Chemical Company). It is also commonly referred to as polyethylene glycol (PEG), which PEG is generally used for lower molecular weight samples. The PEO/PEG monomer (-O-CH<sub>2</sub>-CH<sub>2</sub>-) is composed of carbon (C), hydrogen (H), and oxygen (O) molecules, and it has a molar mass of 44.1 g/mol. It has three bonds per monomer ( $n_o = 3$ ); two (C-O) bonds and one (C-C) bond. The C-C and C-O bonds lengths ( $l_o$ ) are 1.54 Å (0.154 nm) and 1.43 Å (0.143 nm), respectively. In subsequent calculations the average bond length of the monomer is required, which since there are two C-O bonds and one C-C bond the average bond length for PEO is  $l_o = 1.47$  Å. The bond strength of the C-O and C-C bonds have been theoretically derived to be 4.1 and 4.3 nN (Grandbois et al., 1999), respectively. These estimates are consistent with previous studies that have estimated the bond strength based on the onset of chain scission degradation of PEO in pipe flows (Vanapalli et al., 2006; Elbing et al., 2009). Thus, the average bond strength of the PEO monomer is estimated to be 4.2 nN.

The current study primarily uses a single PEO with a manufacturer specified molecular weight ( $M_w$ ) of 4,000,000 g/mol (POLYOX WSR-301, Dow Chemical Company). However, other activities related to this project use samples with mean molecular weights of  $0.6 \times 10^6$  g/mol (182028, Aldrich),  $1.0 \times 10^6$  g/mol (372781, Aldrich),  $2.0 \times 10^6$  g/mol (372803, Aldrich), and  $8.0 \times 10^6$  g/mol (372838, Aldrich). All of these polymers were supplied as a dry white powder, which is then mixed with water to produce stock polymer solutions at desired concentrations.

## **2.2 Preparation Process**

When it comes to reliable scientific investigation, consistency of data is key. In the case of polymer studies, if the polymer in question is not properly mixed, it can lead to degradation of the polymer chains, reducing the effectiveness for drag reduction (Elbing et al., 2009; 2011) and skew the results, possibly even leading to false results, since both lower concentrations and lower molecular weights produce less drag reduction. Thus, this work seeks to identify a robust method of preparation that results in a consistent and accurate batch of polymer solution at a desired concentration.

In general, a master (stock) solution is made, from which other solutions are diluted and tested. For this study, the master solutions were prepared in 15 kg batches at a polymer concentration ( $C$ ) of 400 ppm. The calculation of polymer concentration, for both dilute and master solutions, is calculated using equation (2.1), shown below.

$$C = \frac{m_{polymer}}{m_{solution}} * 10^6, \quad (2.1)$$

Here  $m_{polymer}$  and  $m_{solution}$  are the masses of the polymer powder and final solution, respectively. In general, the  $m_{solution}$  includes the mass of the polymer plus the added water mass, but unless preparing samples at high concentrations (>1000 ppm) this has a negligible impact (~0.1% error at 1000 ppm).

See Appendix A for a more detailed description of the polymer preparation procedures, but here the basic steps are highlighted:

- The desired amount of PEO is measured into a beaker (6 g of PEO for the 15 kg batch of 400 ppm). For the current study, the polymer was measured on a 150-gram digital scale (ED-150 Symmetry, Cole-Parmer, Vernon Hills, IL, USA), which has an accuracy of 0.02 grams.
- Add a pinch (approximately  $\frac{1}{4}$  to  $\frac{1}{2}$  gram) of sodium thiosulfate ( $\text{Na}_2\text{S}_2\text{O}_3$ ), hereafter referred to as STS (217263, Sigma-Aldrich, Darmstadt, Germany). The STS is used to neutralize any chlorine that might be in the water supply, as chlorine can rapidly degrade PEO when in solution with water. STS residue and the products of its reaction with chlorine have been shown to have a negligible impact on polymer drag reduction (Petrie et al., 2003; Elbing et al., 2011).
- The PEO powder was then mixed with water, which this is a critical step with several nuances and it is recommended that anyone following these instructions read the detailed discussion in Appendix A. The ultimate objective is create a final master solution at a desired concentration with no aggregates.
- Once the mixing is complete, the polymer/water solution must be left to fully hydrate. The master solutions were covered, sealed, and allowed to hydrate for approximately 12-16 hours before use (higher the concentration the longer the recommended hydration time).

Generalizing some of the observations in Appendix A for PEO solution mixing suggests that approximately  $\frac{1}{3}$ <sup>rd</sup> of the total added water should be evenly divided between the initial fill and the final rinse/dilution. Thus leaving  $\frac{2}{3}$ <sup>rd</sup> of the added water for the adding of the PEO powder. This implies that for every kilogram of water added one needs to add 0.0015C grams of

PEO, where  $C$  is the concentration in ppm. From experience (Elbing, 2009), this is a good target though the cumulative  $1/3^{\text{rd}}$  of the added water for the initial and final steps needs to be reduced for concentrations above  $\sim 1000$  ppm. This sets a nominal upper limit of 1.5 grams of PEO per kilogram of water for the rate at which PEO powder should be directly hydrated into water. This would limit the maximum batch concentration to 1500 ppm, but higher concentrations are possible (large batches of 6000 ppm were prepared in Elbing et al. (2011)) though with the requirement that the solution be given at least 24 hours before use to dissolve the polymer aggregates into the solution.

### ***2.3 Limitations and Recommendations for Preparation Method***

The end goal is homogeneously mixed PEO solution with a water solvent. Based on experience from the current work as well as previous research, there are some important items that one should consider when gently sprinkling the contents of the beaker into the jet:

- (1) It is imperative that any polymer leaving the beaker ends up in the bucket with the water to ensure the accuracy of the final solution concentration. There is a tendency, even with the precautions given, for some of the polymer to wind up on the end of the nozzle, primarily due to the blowback mist previously mentioned. To date, a way to completely avoid this has not been determined. However, the effect can be mitigated by sprinkling the powder into the jet several inches downstream from the nozzle exit and keeping the angle of the jet at  $\sim 45^\circ$  from the horizontal
- (2) While moving the location that the powder is sprinkled into the jet farther from the tip helps mitigate the issue with polymer building up on the nozzle, there is a limit to how far downstream one can add the powder. Too far away and the water nozzle and the jet begins breaking down into dispersed droplets. This is problematic since some

of the powder could miss the jet and land on the free surface, which would form a very large agglomeration on the surface. While the exact location is dependent on the flowrate, for the current work a good nominal target was to sprinkle near the centroid of the triangular jet.

- (3) Under no circumstances should metal be used to mix the polymer solution.

According to McGary (1960) and supported by observations made in the EFPL for the current work, the degradation rate of PEO is accelerated in the presence of certain metals. One of the original methods of mixing PEO/water solutions in the current work used a 10-gallon plastic gravity fed tank (3687K102, McMaster-Carr) with a high carbon steel/chrome-vanadium-steel double box mixer (G02111, Goldblatt Tool Company). When using the metal stirring rod, all master solutions were completely degraded to the point where their characteristics mimicked that of water. While McGary (1960) did not include this metal in their study, based on this previous work it was hypothesized that the metal from the stirrer was causing the accelerated degradation. Consequently, a new PEO mixing procedure was formed that did not utilize the metal stirrer (i.e. the procedure listed above) to test this hypothesis. Results from this testing are presented in Figure 1, and this new prescribed mixing method has resulted in consistently stable master solutions. Both samples were allowed to settle for 5 hours before testing. Within 16 hours, the solution mixed with the metal stirring rod degraded by almost 25%.

- (4) Numerous factors can directly affect the amount and rate of degradation in a PEO/water solution. Based on previous work (McGary, 1960; Afifi-Effat & Hay, 1971; Layec & Layec-Raphalen, 1983; Han et al., 2017), some of the primary factors that directly affect the quality and degradation rate of the polymer includes, but not limited to, the age of the PEO/water solution, UV light, pH level, temperature, oxidizers, heavy metals, and bacteria in the water. Based on their work, polymer

solutions should be mixed with as pure of water as possible, in dim light, and in a temperature controlled environment.

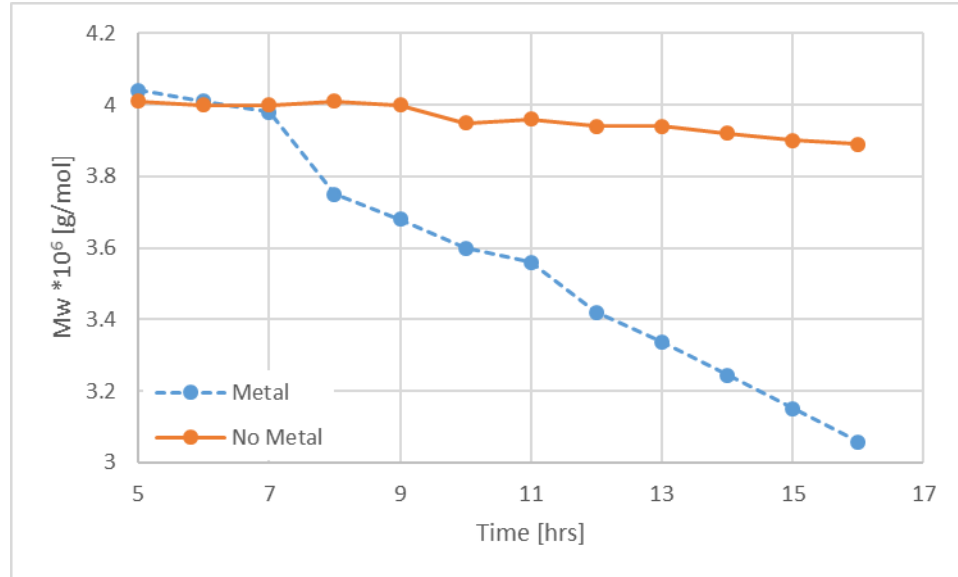


*Figure 1. A demonstration of how the molecular weight of a polymer solution degrades in the presence of metal.*

Given the above observations, it is recommend that once the PEO/water solution is fully hydrated that it be used as soon as possible. In the current work, the master solution was completely degraded (i.e. behaved like water) after about 2 days (48 hours). However, it should be noted that in Elbing (2009) stable master solutions were stable for over 200 hours, but those master solutions were stored in large sealed, non-transparent reservoirs until use.

## CHAPTER III

### POLYMER CHARACTERIZATION

#### **3.1 Molecular Weight**

##### *3.1.1 Measurement approach*

The drag reduction performance is very sensitive to the molecular weight and concentration of the prepared solutions. Given the numerous potential degradation mechanisms and uncertainty of the master solution concentration, it is critical that an independent means of quantifying each are performed. Gel permeation chromatography (GPC) is the ideal means of measuring the molecular weight in polymer solutions, but at these high  $M_w$  the GPC method becomes impractical for several reasons including that it is isorefractive in tetrahydrofuran (THF), one of the most common eluents. Vanapalli et al. (2005) developed an alternative approach for PEO by identifying a correlation in data compiled in Virk (1975) between the shear-rate at the onset of drag reduction ( $\gamma^*$ ) and the PEO molecular weight, shown in equation 3.1,

$$\gamma^* = (3.35 \times 10^9) M_w^{-1}. \quad (3.1)$$

The onset of drag reduction and the corresponding shear rate can readily be identified with a pressure drop apparatus, which is commonly referred to as a Virk tube after the pioneering efforts of P.S. Virk (Virk et al., 1967; 1970; Virk, 1975) with similar apparatuses. The Virk tube is simply a straight section of pipe with fully developed flow, which makes pressure drop across a given length of tube directly proportional to the skin-friction over that length.

The Virk tube works on the concept that in fully developed flow the mean velocity profile no longer changes with downstream distance, as illustrated in

Figure 2. Applying a CV that encloses the fluid in the pipe from  $x_1$  to  $x_2$  and assuming the flow is steady, reduces the conservation of mass to

$$\frac{dM_{sys}}{dt} = 0 = \int_{outlet} u_{out} dA - \int_{inlet} u_{in} dA, \quad (3.2)$$

which is equivalent to stating that the velocity profile does not change ( $u_{in} = u_{out}$ ) since the area is constant. Now applying conservation of momentum in the  $x$ -direction produces

$$\sum F_x = \int_{outlet} u_{out}^2 dA - \int_{inlet} u_{in}^2 dA = 0. \quad (3.3)$$

Here the sum of the forces in the  $x$ -direction ( $F_x$ ) equals zero since conservation of mass showed that  $u_{out} = u_{in}$ . Since the pipe is horizontal, there is no body forces (i.e. neglect gravity). Since there are no constraint forces within the control volume (i.e. the control volume boundary does not cut through any solid surfaces), the remaining external forces (pressure differential and viscous) must balance each other. The skin-friction (viscous) force is equal to  $F_f = \tau_w(\pi d)\Delta x$ , where  $\tau_w$  is the wall shear stress,  $d$  is the inner diameter of the pipe, and  $\Delta x$  is the length between the inlet and outlet. This viscous force acts in the negative  $x$ -direction and must be balanced by the pressure differential force,  $F_{\Delta p} = (p_{in} - p_{out})(\pi d^2/4)$ , where  $p_{in}$  and  $p_{out}$  are the inlet and

outlet pressures, respectively. Therefore, conservation of momentum for fully developed pipe flow reduces to  $F_f = F_{\Delta p} = \tau_w(\pi d)\Delta x = \Delta p(\pi d^2/4)$ , which can be rearrange to solve for the wall shear stress,

$$\tau_w = \frac{d \Delta p}{4 \Delta x}. \quad (3.4)$$

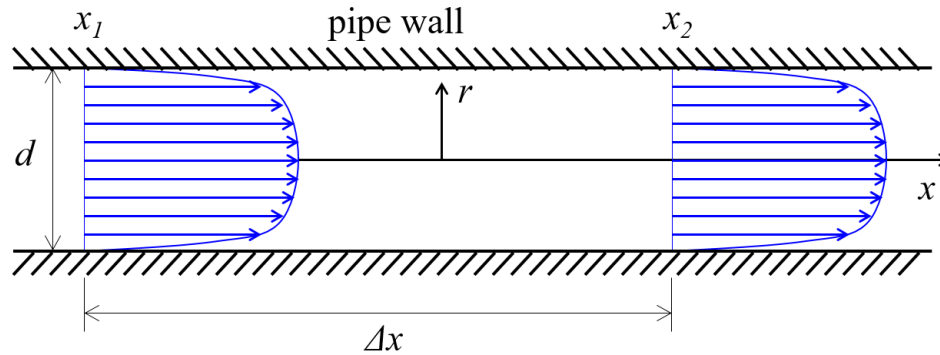


Figure 2. Sketch of fully developed turbulent pipe flow, which is required to relate the pressure drop within the Virk tube with skin-friction.

After the preparation of the master solution has been completed, it must be checked for degradation. According to the Dow Chemical Company, the approximate molecular weight (Mw) of PEO WSR-301 is 4 million g/mol. As such, a way to test the effectiveness of the preparation procedures given above is to check the molecular weight.

### 3.1.2 Virk tube design

For the current work, a Virk tube was constructed from instrument grade 316 stainless steel seamless tubing (SS-T8-S-035-20, Swagelok, Solon, Ohio, USA) in the Experimental Flow Physics Laboratory (EFPL) at Oklahoma State University. This lab is not pressure or temperature controlled. A schematic of the Virk tube is shown in Figure 3. The tubing has an outer diameter

of 12.7 mm (0.5 in) and 0.889 mm (0.035 in) thick walls, which results in an inner diameter ( $d$ ) of 10.9 mm (0.43 in). The lengths of the entrance, test, and end sections were 1.5 m ( $140d$ ), 1.05 m ( $96d$ ), and 0.22 ( $20d$ ), respectively. The test sample was delivered to the tube from an 18.9 liter (5-gallon) 316L stainless steel pressure vessel (740560, Advantec) rated to 0.90 MPa (130 psi). The pressure vessel was pressurized with house compressed air to  $\sim 276$  kPa (40 psi), which then pushed the sample up through a dip tube into a flexible hose that was connected to the Virk tube.

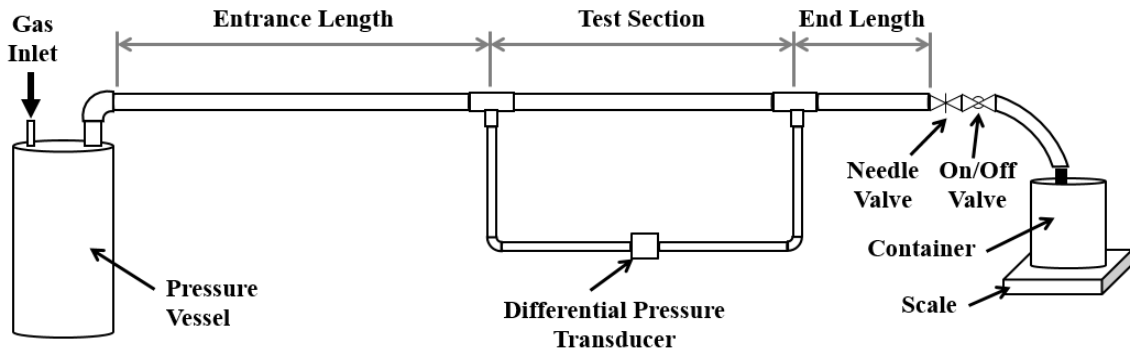


Figure 3. Schematic of the Virk tube (pressure drop apparatus) used for characterization of the polymer batches.

A differential pressure transducer (PX2300-5DI, Omega Engineering, Stamford, CT, USA) was connected between the inlet and the outlet of the test section to measure the  $\Delta p$  from equation (3.4) (note that  $\Delta x$  is the length of the test section, 1.05 m). The 4-20 mA output from the pressure transducer was passed through a 250  $\Omega$  wire-wound ceramic resistor (CW series, Vishay) as illustrated in Figure 4, which the voltage across this resistor was recorded via a data acquisition card (USB-6218-BNC, National Instruments) and commercial data acquisition software (LabView15.0.1f7, National Instruments, Austin, TX, USA). The water temperature was measured with a 25-125  $^{\circ}\text{F}$  thermometer (Tel-Tru Manufacturing Co., Rochester, NY, USA), which has a 1  $^{\circ}\text{F}$  resolution. The mass flowrate cannot be measured with traditional flowmeters

because they generally require an assumption of a Newtonian fluid. Thus, the mass flowrate was measured via timing the period with a stopwatch (RS-013, ProCoach) required to fill a container (5-gallon bucket) with a given mass of polymer solution. The solution mass exiting the Virk tube was measured on a 35-kg digital bench/floor industrial scale (CPWplus-35, Adam Equipment Inc, Oxford, CT, USA).

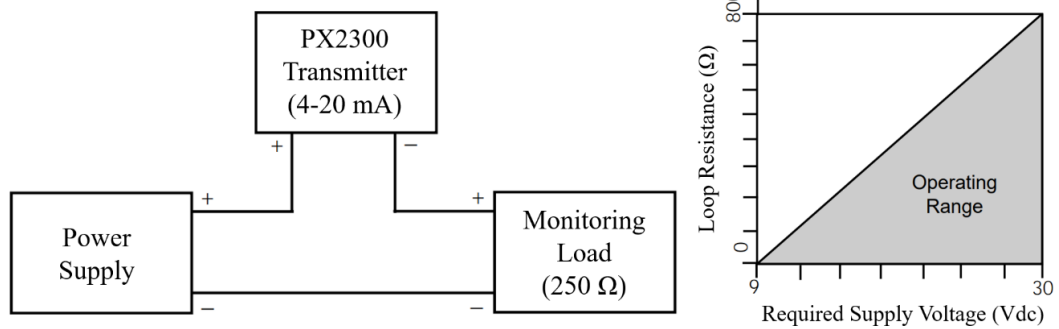


Figure 4. (left) Wiring diagram for the PX2300 pressure transducer. The voltage across the monitoring load is what is recorded by the data acquisition system. (right) Graph of the minimum required supply voltage for a given loop resistance. If minimum voltage is not supplied the performance is unpredictable. Both illustrated are adapted from Omega Engineering (1999).

### 3.1.3 Test procedures

It is recommended that at least once a month the pressure transducer calibration be confirmed. Given the low differential pressure range (5 psi), the best method for checking the calibration is using hydrostatic pressure. Here a tube is attached the high-pressure side of the pressure transducer and filled with varying elevations of water while the low-pressure side is open to atmosphere. The output voltage recorded on the data acquisition system is then plotted versus the hydrostatic pressure ( $\rho gH$ ), where  $\rho$  is the water density,  $g$  is gravitational acceleration, and  $H$  is the height of the water above the centerline of the pressure transducer inlet/outlet (make sure the pressure transducer is horizontal). It is also important that the wiring be identical between

the calibration and testing with the Virk tube, as any change in the wiring could change the resistance in the loop, which would alter the voltage across the resistor.

It is important that the pressure transducer (PT) and the connecting wires remain dry. In a case where they were not, the system should not be used until they are dried. Afterwards, the bolts securing the PT are checked. It is important the PT be secure against even small motions, which can introduce error in the voltage measurements. Securing the PT minimizes movement, allowing for reliable measurements.

Next, all wires and electrical contacts within the system are checked for a secure, tight connection. This included checking electrical contacts as well as checking the wire shielding. When inspecting the system, the state of the wire ends was also noted. For example, if a wire only had a small number of contacts with the screws holding the wire in place, it was replaced. Wires with noticeable damage to the shielding were replaced, and loose electrical contacts were tightened. If anything was tightened, replaced, or cleaned, this was noted in the laboratory notebook. If there was a significant change in the wiring, then the pressure transducer calibration should be repeated.

The pressure vessel is initially filled with water that is used to (i) flush the system, (ii) bleed the pressure transducer lines, and (iii) confirm that the Virk tube is operating as expected. Flush of the system with water is recommended between individual samples to minimize the potential of the current data being contaminated by the previous sample. Specifics on bleeding the transducer lines are discussed subsequently when discussing polymer sample testing, but the lines should be bled anytime air has entered the system. Finally the water results are compared with the established Newtonian turbulent flow curve (Prandtl-Karman or Blasius law),

$$\frac{1}{\sqrt{f}} = 4.0 \log_{10}(Re\sqrt{f}) - 0.4. \quad (3.5)$$

Here  $f$  is the Fanning friction factor and  $Re$  is the pipe-diameter based Reynolds number. This allows for the accuracy of the setup to be quantified and identification of any potential issues before testing the polymer samples. It is also recommended that this step be repeated at the conclusion of testing for the above reasons as well as establishing confidence that the setup was unchanged during the polymer testing.

Now with the system depressurized and water emptied from the pressure vessel (hereafter referred to as “PV”), the diluted mixture of water and polymer solution from the 400 ppm master solution is added to the PV. For the current work, 0.68 kg of the master solution was diluted with 17.32 kg of additional water, which produced a final solution with a concentration of approximately 15 ppm. In general, the ratio of the diluted concentration ( $C_{diluted}$ ) to the master batch concentration ( $C_{master}$ ) is equal to the mass of the master solution ( $m_{master}$ ) divided by the sum of the mass of the batch and added water ( $m_{add}$ ),

$$\frac{C_{diluted}}{C_{master}} = \frac{m_{master}}{m_{master} + m_{add}}. \quad (3.6)$$

For example, to create a total of 18 kg of a 10 ppm diluted sample from the 400 ppm master solution, one would add 0.45 kg of the master solution ( $m_{master} = (m_{master} + m_{add}) C_{diluted}/C_{master} = (18 \text{ kg})(10/400) = 0.45 \text{ kg}$ ) to 17.55 kg of water ( $m_{add} = 18 \text{ kg} - m_{master} = 17.55 \text{ kg}$ ).

Kalashnikov (1998) showed that the drag reduction performance did not depend upon whether the sample was prepared by diluting a master solution or by preparing the sample at the desired concentration to be tested. However, it is important the diluted sample be a homogeneously mixed solution. When diluting a sample in the PV, the PV was first filled until it contained 10 kg

of water, and afterwards, the appropriate amount of the master solution was added. To aid in making a homogeneous dilution, the hose used to fill the PV is held so that the stream of water splashes against the sidewall of the PV. This is done so the momentum of the water will carry it along the curvature of the PV, giving it a rotational motion as it falls into the solution. This creates a swirling, mixing motion as illustrated in Figure 5, which helps ensure that the diluted sample was mixed evenly. However, some caution should be given here since if the swirl and/or jet is too high it can promote shear degradation of the polymer sample. The PV is filled until it contains 18 kg of solution. Then it is seal and allowed to rest for about 10 minutes. The temperature of the solution should be measured and recorded.

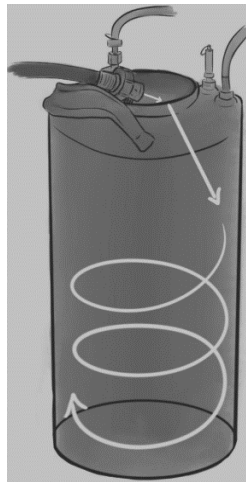


*Figure 5: Illustration of how to use the swirling motion of the water to mix the polymer solution with water while diluting. Drawn by Haylie "Reese" Hadzeriga.*

Once the diluted sample was prepared, the system was pressurized to 276 kPa (40 psi) to begin the bleeding process. The shutoff valve on the far end of the Virk tube was opened to push the majority of the air out of the tube and allow the tube to fill with solution. Once there is a steady stream of solution exiting the tube (i.e. no air is observed exiting the tube), the shutoff

valve is closed. The PT has 3 screws used for bleeding the pressure ports (illustrated in Figure 6): one (1) screw on the high-pressure side and two (2) vertically aligned screws on the low-pressure side. To bleed the pressure transducer, the high pressure screw (one of the flat surface) is opened a maximum of 2 turns, and then all the air in the clear tube attached to that side of the PT was allowed to bleed out. Once all visible air-bubbles were gone, that side was allowed to bleed for an additional 10 seconds before the screw was tightened back up. The same procedure was followed for the low-pressure screws, except they were opened at the same time. After the PT tubes are bled, the shutoff valve was opened again for a few seconds to allow any small amounts of air in the entrance to the PT tubes to be expelled.

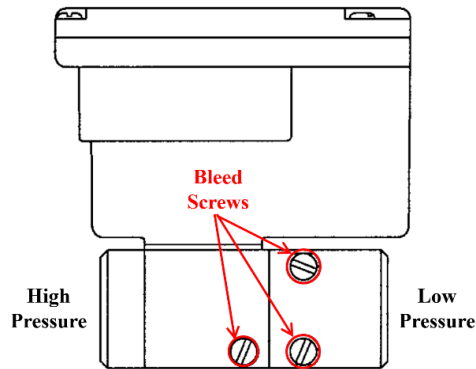


*Figure 6. Schematic of the pressure transducer (PX2300, Omega Engineering) illustrating the location of the bleed screws. This illustration is adapted from the PX2300 user manual (Omega Engineering, 1999).*

After the above steps were completed, the system was ready for testing. Equipment required for data acquisition includes a stopwatch, 2 of the 5-gallon buckets, the 35-kg digital scale (CPWplus-35, Adam Equipment), and data acquisition system as described previously. Specifics of the instrumentation and data acquisition system are provided above, but here the focus is on the specific procedures required to acquire the data.

One of the 5-gallon buckets was placed on the digital scale, and the scale was tared to subtract the weight of the bucket. The second 5-gallon bucket was placed on the floor next to (though not touching) the digital scale. The bucket on the scale will be referred to as B1 while the second bucket next to the scale will be referred to as B2 for clarity. At this point the LabView data acquisition program was started and set to record data at 150 Hz. The data acquisition was allowed to record for ~30 seconds (minimum) before making any changes to the setup (e.g. opening the valve to start flow). This static period, where no interaction with the Virk tube takes place, allows the user to establish an accurate zero pressure differential voltage ( $V_{zero}$ ). Note that a similar period of time of rest was recorded after collecting a given flow condition, which if there is a significant variation in  $V_{zero}$  it would indicate that the given condition is likely erroneous. In addition, tracking  $V_{zero}$  through the course of an experiment provides a check as to whether anything was altered with the wiring and/or damage to the pressure transducer.

When ready to test a given condition, the clear exit tube of the Virk tube was held by the user above B2, the shutoff valve of the Virk tube was opened, and polymer solution would begin flowing out. Once the flow is at steady state (i.e. few seconds to allow the flow to stabilize), the flow was quickly switched to B1 on the digital scale. Simultaneously, the stopwatch is started, which it is recommended that the same person start the stopwatch and switch the flow from B2 to B1. This is because a nontrivial amount of uncertainty is introduced with the use of the second person because their reaction time is a bias error on the time measurement. Once over B1, the polymer solution continues to flow into B1 until ~1 kg of solution has been gathered. Keep the mass nearly constant rather than the time reduces measurement uncertainty, especially at low flow rates. It is also important that while gathering data, the exit tube does not move. This is because any elevation change at the tube exit changes the losses in the system, which in turn alters the flow rate. Thus if the exit tube is being moved it creates uncertainty in the mass flow

rate as well as an increase in the uncertainty in the measured pressure voltage (i.e. slight movements are readily observed in the pressure measurement).

Once the scale reads ~1 kg, simultaneously, the exit tube of the Virk tube was moved back to B2 and the stopwatch was stopped. Then the shutoff valve is closed, which is done to maximum the number of test conditions possible for a given batch of polymer solution. The mass readout from the scale and the time readout from the stopwatch were recorded as “Run #”. Additionally, any observations about the test condition of the flow were recorded (e.g. if there were unusual vibrations in the tube, stuttering flow, or a mistiming between tube movement and firing of the stopwatch). An example of a typical data recording during the experiment is provided in Table 1.

*Table 1: Example data table for recording data during experimentation.*

<b>Date: 03/17/2017    Operator(s): Name    Temperature (°F): 70    Pressure (psi): 40</b>			
<b>Measurements</b>			
<b>#</b>	<b>Mass (kg)</b>	<b>Time (s)</b>	<b>Error?</b>
<b>1</b>	1.23	10.28	
<b>2</b>	4.56	10.16	
<b>3</b>	7.89	10.02	
<b>4</b>	2.34	9.86	*

It is recommended that after each data point, an initial data processing be performed that allows the collected data point to be plotted on a Prandtl-Karman (PK) plot. This allows the user to have an educated guess about whether the next condition should be acquired at a higher or lower speed. The mass flow rate of the Virk tube was then adjusted up or down as desired using a gate valve located upstream of the shutoff (on/off) valve (see Figure 3). Then a small period of non-interaction was allowed to establish a new  $V_{zero}$ . The above process was repeated until the desired number of data points were gathered or until the PV was exhausted of its supply of polymer solution. Once all data was acquired, the system was flushed with water again. While the

system was still pressurized, the entire Virk tube was drained and bled of all fluid. Finally, the pressure vessel was opened and valves opened to allow the entire system to dry (i.e. it is not recommended to leave the system with liquid and/or closed as it can promote corrosion and equipment damage).

### 3.1.4 Data reduction

Given the process laid out earlier in this paper, multiple test conditions are acquired as a voltage signal and analyzed alongside the corresponding mass, time, and temperature data for each test condition. Figure 7 shows an example of a recorded voltage signal during two test conditions. Two test conditions are apparent from the high (elevated) voltage reading above the  $V_{zero}$  level, which is the measurement voltage  $V_{measure}$ . Thus each test condition consists of two distinct regions: (1) a preceding low region at  $V_{zero}$  and (2) a proceeding high region at  $V_{measure}$ . A clear cut separation line can be seen between regions, which occurs due to the physical opening and closing of the Virk tube during data acquisition. When the signal changes specifically from a high region to a low region, this is taken as the end of a test condition.

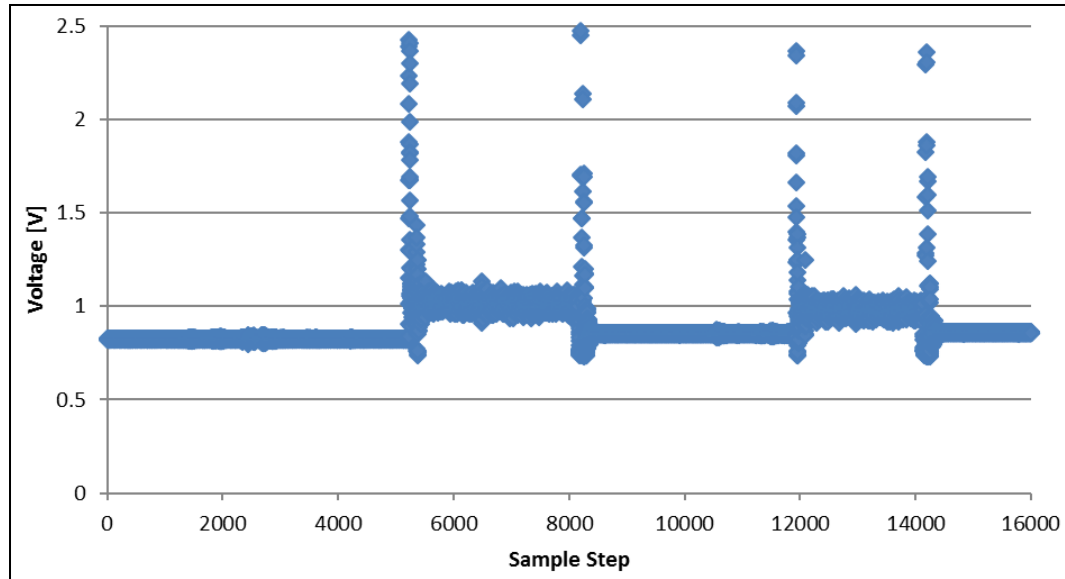


Figure 7: Raw voltage output of two test conditions during DAQ. There are two clear upper and lower regions of the signal data. The lower region ( $V_{zero}$ ) corresponds to the no-flow condition, and the upper region ( $V_{measure}$ ) is when there is a working fluid flowing through the Virk tube. When the signal changes from an upper region to a lower region, this is considered the end of that test condition.

Data reduction was performed in Excel with each test condition isolated and zoomed in so that  $V_{zero}$  and  $V_{measure}$  ranges could be accurately identified. Using this method, an approximate cell address for the beginning and end of each region of interest was determined. Using these ranges, an average of all values within that range was determined resulting in  $\bar{V}_{measure}$  and  $\bar{V}_{zero}$ . Special attention must be paid to each region, as only a stable voltage signal is considered for analysis. Figure 8 below shows a zoomed in view of a  $V_{measure}$  period, and it can be seen that the signal behavior takes a short moment to stabilize. Only the stable region is considered for analysis. Also of note, it is critical that the same period of time used to measure the mass flow rate is used for the average measurement voltage. For this reason, it is recommended to actually make a significant movement of the exit tube when switching between B1 and B2 to clearly locate these measurement period.

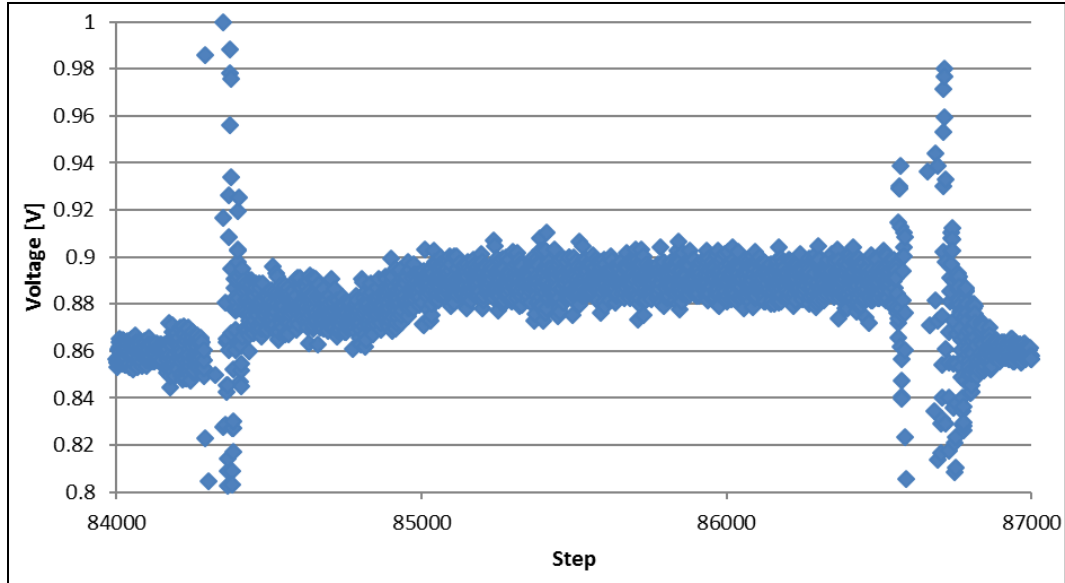


Figure 8: Zoomed in raw voltage output, demonstrating how a  $V_{measure}$  signal cannot be analyzed entirely. After a certain amount of time the  $V_{measure}$  has stabilized to its true value.

This data reduction process is tedious to do by hand and can lead to user errors. Consequently, a VBA program was created to automate the data reduction process. The user simply loads in a data set, types the test conditions (mass, time, and temperature), and then identifies the start and end locations. Afterwards, the VBA code allowed the user to click individual low and high points for both  $V_{zero}$  and  $V_{measure}$  on the chart, and then average the all the points between the low and high points for each region. The code for this process has been included in Appendix B – Analysis Code. To reiterate, the main purpose of this code was only to reduce the amount of time it took to perform the data reduction.

### 3.1.5 Data analysis and calculations

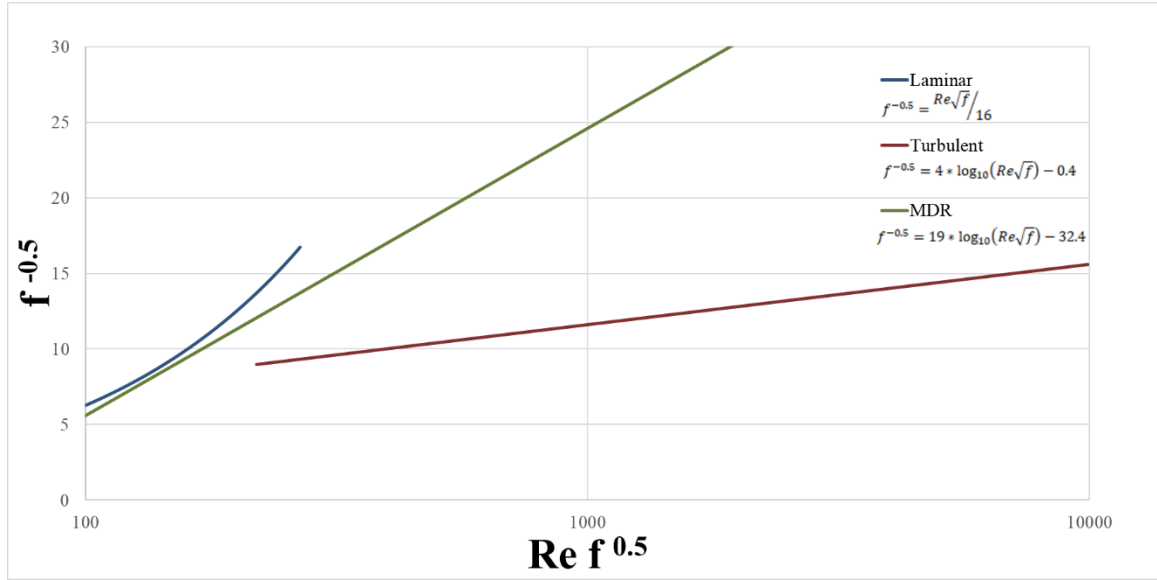


Figure 9: PK plot showing the relationship between the Fanning friction factor and the pipe diameter based Reynolds Number. Lines corresponding to laminar flow, turbulent Newtonian flow (PK law), and the empirically derived Maximum Drag Reduction (MDR) limit (Virk, 1975).

After the data reduction for each test condition was processed, the reduced data were plotted on a PK plot. Figure 9 provides an example PK plot that includes lines for laminar flow, turbulent Newtonian flow (PK law), and an empirically derived maximum drag reduction (MDR) limit (Virk, 1975). All data of interest should fall between the PK law (Newtonian turbulent flow) and MDR. Any data points that were not “trusted” or outside the polymeric range (i.e. below onset of drag reduction) were removed, and then the remaining data were fit to a logarithmic trend line. The equation defining this trend line takes the form of

$$f^{-0.5} = A \log_{10}(Re\sqrt{f}) + B, \quad (3.7)$$

where  $A$  is the slope and  $B$  is the y-intercept. The onset of drag reduction is identified by determining the intersection of this logarithmic trend line with the PK law given in equation (3.5), which the onset of drag reduction is related to the  $M_w$  via equation (3.1). The intersection (i.e. the

onset of drag reduction) is determined by setting  $(f^{-0.5})_{water} = (f^{-0.5})_{polymer}$ . Using ‘\*’ to denote that this defines the onset of drag reduction condition, this implies

$$\left(\frac{1}{\sqrt{f}}\right)_{water}^* = \left(\frac{1}{\sqrt{f}}\right)_{polymer}^* = 4.0 \log_{10}(Re\sqrt{f})^* - 0.4 = A \log_{10}(Re\sqrt{f})^* + B. \quad (3.8)$$

This can be rearranged to solve for  $Re\sqrt{f}$  at the onset of drag reduction,

$$(Re\sqrt{f})^* = 10^{(B+0.4/4-A)}, \quad (3.9)$$

which given  $(Re\sqrt{f})^*$  the corresponding  $1/\sqrt{f}^*$  is readily found by inserting the computed  $(Re\sqrt{f})^*$  into the PK law. Then Reynolds number and Fanning friction factor at the onset of drag reduction are determined from  $Re^* = (Re\sqrt{f})^* (1/\sqrt{f})^*$  and  $f^* = \{(1/\sqrt{f})^*\}^{-2}$ , respectively.

Finally, the shear rate at the onset of drag reduction is determined from the definition of the Fanning friction factor,

$$f^* \equiv \frac{\tau_w^*}{0.5\rho U^2} = \frac{\nu \gamma^*}{0.5U^2} \rightarrow \gamma^* = \frac{U^2}{2\nu} f^*. \quad (3.10)$$

Here  $\tau_w^*$  ( $= \rho \nu \gamma^*$ ) is the wall shear stress at the onset of drag reduction,  $\rho$  is the fluid density,  $U$  is the average velocity in the pipe,  $\nu$  is the kinematic viscosity, and  $\gamma^*$  is the shear rate at the onset of drag reduction that is used in equation (3.1) to estimate the mean molecular weight.

### 3.1.6 Uncertainty analysis

When making measurements with use of the stopwatch, uncertainty can arise due to human error. To quantify the uncertainty in the time measurement due to human error, 15 trials were performed where the user would try to stop the stopwatch as close to 10 seconds as possible. Afterwards, the standard deviation ( $\sigma$ ) and the average of the 15 trials were computed. The resulting uncertainty in the time measurement was calculated as

$$\epsilon_t = \sqrt{(d_{watch})^2 + (t_{avg} - t_{target})^2 + (\sigma_{Time})^2}, \quad (3.11)$$

where  $d_{watch}$  is the resolution of the stopwatch display,  $t_{avg}$  is the average of the 15 trials,  $t_{target}$  is the target period (10 seconds), and  $\sigma_{time}$  is the standard deviation of all the trials. The difference between the target and average values was meant to quantify the reaction time of the user while the standard deviation quantified the random errors associated with stopping the stopwatch. The random errors would have been more appropriately performed while acquiring data, but a fixed time period is not ideal for data collection.



Figure 10: Simple sketch demonstrating the potential uncertainty introduced by a dip (warp) in the measuring tape used when measuring the length of the Virk tube measurement section. The tape measure would be measuring  $2C$  while the actual length was  $L$ .

There is also uncertainty that arises due to the temperature measurement, which ultimately impacts the accuracy of the fluid properties. Since the resolution of the thermometer is  $1^\circ\text{F}$ , the uncertainty of the temperature measurement  $\epsilon_{temp}$  was taken as  $\pm 0.5^\circ\text{F}$ . Furthermore, uncertainty can arise from the accuracy of the measurement of the distance between the pressure taps (holes) in the Virk tube. Primary sources of uncertainty are the tape measure resolution ( $d_{tape}$ ), hole-center accuracy ( $d_{hole}$ ), and potential warping of the tape measure during the measurement. The last source is approximated assuming the largest dip in the tape measure would be at the center and the dip would be within an eighth of an inch (3.2 mm), which estimates the deviation between the measured length ( $2C$ ) and the actual length ( $L$ ). The computation of  $C$  is

illustrated in Figure 10. Thus the resulting uncertainty in the measurement of the distance between the pressure taps ( $\Delta x$ ) is

$$\epsilon_{\Delta x} = \sqrt{(d_{tape})^2 + (a_{hole})^2 + (2C - L)^2}. \quad (3.12)$$

Uncertainty can also be introduced when measuring out the total mass of dry polymer used in the solution due to the scale. Many factors such as age, damage, or even quality control errors can result in uncertainty. To qualify the uncertainty of the Cole-Parmer scale, a set of weights with known masses were placed on the scale in increasing increments, and the mass readout of the scale was recorded. This process was repeated 3 times, generating the data presented in Table 2.

*Table 2: Cole-Parmer digital scale uncertainty measurement data.*

Mass (g)	Read 1 (g)	$\Delta 1$ (g)	Read 2 (g)	$\Delta 2$ (g)	Read 3 (g)	$\Delta 3$ (g)	Avg (g)	Avg $\Delta$ (g)
0	0.00	0.00	0.01	-0.01	0.00	0.00	0.00	0.00
20	19.97	0.03	20.00	0.00	20.03	-0.03	20.00	0.00
40	39.99	0.01	39.98	0.02	40.00	0.00	39.99	0.01
50	50.02	-0.02	50.01	-0.01	50.00	0.00	50.01	-0.01
70	70.05	-0.05	70.06	-0.06	70.05	-0.05	70.05	-0.05
90	90.01	-0.01	90.02	-0.02	90.00	0.00	90.01	-0.01
100	100.04	-0.04	100.04	-0.04	100.04	-0.04	100.04	-0.04
120	120.04	-0.04	120.04	-0.04	120.06	-0.06	120.05	-0.05
140	140.07	-0.07	140.08	-0.08	140.08	-0.08	140.08	-0.08
150	150.06	-0.06	150.06	-0.06	150.08	-0.08	150.07	-0.07
	<b>Std. Dev.</b>	3.24E-02	<b>Std. Dev.</b>	3.13E-02	<b>Std. Dev.</b>	3.31E-02	<b>Std. Dev.</b>	3.06E-02
	<b>Average</b>	-2.50E-02	<b>Average</b>	-3.00E-02	<b>Average</b>	-3.40E-02	<b>Average</b>	-2.97E-02

In Table 2, the “Mass” column is the target mass specified by the calibration weights. The “Read” columns are the readout on the digital display of the Cole-Parmer scale, and the “ $\Delta$ ” columns are the signed difference between the target and readout (signed to preserve readouts both above and below). From these 3 trials, two average columns are calculated. The “Avg”

column is the average of the 3 scale readouts, and the “Avg  $\Delta$ ” is the difference between the target mass and the average readout. From this, the standard deviation of the “ $\Delta$ Avg” is taken, and the overall average of the “Avg  $\Delta$ ” is taken. The Figure 11 shows all 3 trials plotted against each other, as well as against the true mass and the “Avg”. From this figure, it is clear that they align well.

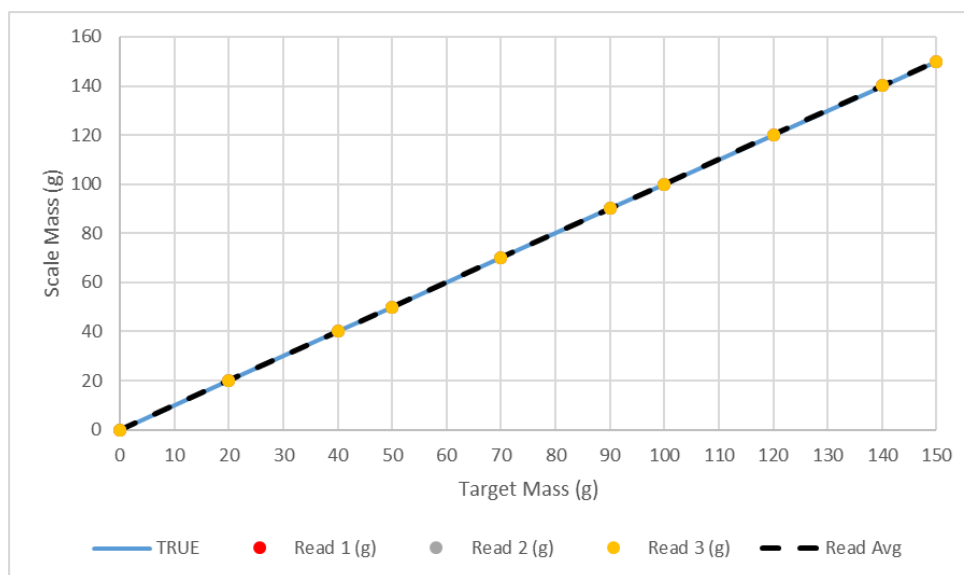


Figure 11: Brief comparison of Cole-Parmer scale data readout vs the target mass value. The dashed line represents the average values of the 3 trials.

However, an additional source of uncertainty was also considered. The glass beaker used to hold and pour the polymer can also be a source of error, as not all the polymer will necessarily transfer out of the beaker completely. A rough way to quantify this is to follow a similar procedure for the scale. The beaker is filled with a certain mass of polymer, and then emptied of polymer. The filled and empty masses of the beaker are recorded, producing Table 3. Here,  $\Delta m$  is the signed difference between the “Emptied Mass” and the “Initial Mass”, and “ $\Delta m$  Avg” is the overall average of the 3 runs. Hence, the uncertainty of the Cole-Parmer scale is

$$\epsilon_{mCP} = \sqrt{d_{CP}^2 + \Delta m_{beaker}^2 + \sigma(m_{actual_i} - Avg_{123,i})^2}. \quad (3.13)$$

Table 3: Cole-Parmer Uncertainty Measurement Data, Beaker Data.

	Run 1	Run 2	Run 3
Initial Mass (g)	51.38	70.97	60.62
Emptied Mass (g)	51.39	70.99	60.61
$\Delta m$ (g)	0.01	0.02	-0.01
	$\Delta m$ Avg (g)	6.67E-03	
	Std.Dev. [ $\Delta m$ ]	1.53E-02	

Table 4: CPWplus-35 Uncertainty Measurement Data, Scale Measurement.

Mass (g)	Read (g)	$\Delta m$ (g)	Mass (g)	Read (g)	$\Delta m$ (g)	Mass (g)	Read (g)	$\Delta m$ (g)	Mass (g)	Read (g)	$\Delta m$ (g)
0.00	0.00	0.00	0.25	0.25	0.00	0.50	0.50	0.00	1.00	1.00	0.00
0.02	0.02	0.00	0.27	0.27	0.00	0.52	0.52	0.00	1.10	1.10	0.00
0.04	0.04	0.00	0.29	0.29	0.00	0.54	0.54	0.00	1.20	1.20	0.00
0.05	0.05	0.00	0.30	0.30	0.00	0.55	0.55	0.00	1.30	1.30	0.00
0.07	0.07	0.00	0.32	0.32	0.00	0.57	0.57	0.00	1.40	1.40	0.00
0.09	0.09	0.00	0.34	0.34	0.00	0.59	0.59	0.00	1.50	1.50	0.00
0.10	0.10	0.00	0.35	0.35	0.00	0.60	0.60	0.00	1.60	1.60	0.00
0.12	0.12	0.00	0.37	0.37	0.00	0.62	0.62	0.00	1.70	1.70	0.00
0.14	0.14	0.00	0.39	0.39	0.00	0.64	0.64	0.00	1.80	1.80	0.00
0.15	0.15	0.00	0.40	0.40	0.00	0.65	0.65	0.00	1.90	1.90	0.00
0.17	0.17	0.00	0.42	0.42	0.00	0.67	0.67	0.00	2.00	2.00	0.00
0.19	0.19	0.00	0.44	0.44	0.00	0.69	0.69	0.00	2.05	2.05	0.00
0.20	0.20	0.00	0.45	0.45	0.00	0.70	0.70	0.00	2.07	2.07	0.00
0.22	0.22	0.00	0.47	0.47	0.00	0.80	0.80	0.00	2.09	2.09	0.00
0.24	0.24	0.00	0.49	0.49	0.00	0.90	0.90	0.00	Std. Dev.		0.00

Additional uncertainty arises from the floor scale (CPWplus-35, Adam Equipment) when measuring out masses transferred into the buckets. Much like the Cole-Parmer scale, a sequence of measurements was taken using known masses and compared against one another, and the empty vs full weights of the buckets were compared as well. Table 4 shows the trial data with  $\Delta m$  defined as the signed difference between the target mass and the scale readout. It can be observed

that the scale is in excellent agreement with the target mass, having a zero standard deviation. In addition, the uncertainty involving the buckets are quantified with the data shown in Table 5. The bucket was weighed empty, filled to 15 kg, emptied, and then weighed again. In this,  $\Delta m_{bucket}$  is defined as the difference between the initial empty weight and the final drained weight. With these values, the uncertainty when using the CPWplus-35 scale was estimated as

$$\epsilon_{m35} = \sqrt{d_{35}^2 + (\Delta m_{bucket})^2}, \quad (3.14)$$

where  $d_{35}$  is the resolution of the scale and  $\Delta m_{bucket}$  is the difference in initial and final masses of the bucket.

*Table 5: CPWplus-35 Uncertainty Measurement Data, Bucket Measurement.*

<b>Bucket Empty Mass (kg)</b>	0.69
<b>Bucket Drained Mass (kg)</b>	0.70
<b><math>\Delta m_{bucket}</math> (kg)</b>	0.01

When considering the uncertain of the area of the pipe in the Virk tube, instrument grade tubing was used. As such, the accuracy of the available instruments available (i.e. caliper) to measure the diameter was assumed larger than the actual diameter uncertainty. Therefore, uncertainty relating to the pipe area and diameter is considered negligible. Note, this was confirmed by the accuracy of the water data using a measured diameter versus the manufacturer specified diameter. This is likely due to the fact that the largest deviations in the diameter from the manufacturer specifications are located at the ends (i.e. where the pipe is cut).

Next, the uncertainty associated with the measured voltages was estimated.

Figure 12 shows a typical voltage signal, which was used to perform the uncertainty analysis of the voltage measurements. There are 26,550 data points in this particular dataset. As defined in

the previous section, low areas are  $V_{zero}$  regions while high areas are  $V_{measure}$ . In this case, there are four  $V_{zero}$  sections and three  $V_{measure}$  sections. First, the average voltage of each  $V_{zero}$  sector is taken, and then those values are averaged together into  $\overline{\Delta V_{zero}}$ . Then, the standard deviation,  $\sigma$ , of the difference between the actual voltage,  $V_{zero}$ , and  $\overline{\Delta V_{zero}}$  were computed. This deviation combined with the pressure transducer resolution ( $d_{PT}$ ) was used to estimate the uncertainty in the zero pressure difference voltage,

$$\epsilon_{V_{zero}} = \sqrt{d_{PT}^2 + \sigma(V_{zero} - \overline{\Delta V_{zero}})^2}. \quad (3.15)$$

A similar approach was taken for the uncertainty of  $V_{measure}$ , but there is also the addition of a  $\Delta V_{zero}$  term,

$$\epsilon_{V_{measure}} = \sqrt{d_{PT}^2 + \sigma(V_{measure} - \overline{\Delta V_{measure}})^2 + \overline{\Delta V_{zero_{i \rightarrow i+1}}}^2}. \quad (3.16)$$

This is to account for how the  $V_{zero}$  baseline could shift between the beginning and end of the measure, ultimately affecting  $V_{measure}$ . Table 6 shows the numerical values for this uncertainty analysis, which when combined gives the estimated uncertainty for the voltage measurement,

$$\epsilon_{\Delta V} = \sqrt{\epsilon_{V_{measure}}^2 + \epsilon_{V_{zero}}^2}. \quad (3.17)$$

Table 6: Voltage Uncertainty Measurement Data

Run	1-2	2-3	3-4	Avg	Std. Dev.
$V_0$	-4.69E-04	6.37E-05	1.33E-04	-9.06E-05	1.29E-03
$V_{measure}$	-8.66E-04	7.72E-03	N/A	3.43E-03	3.89E-02

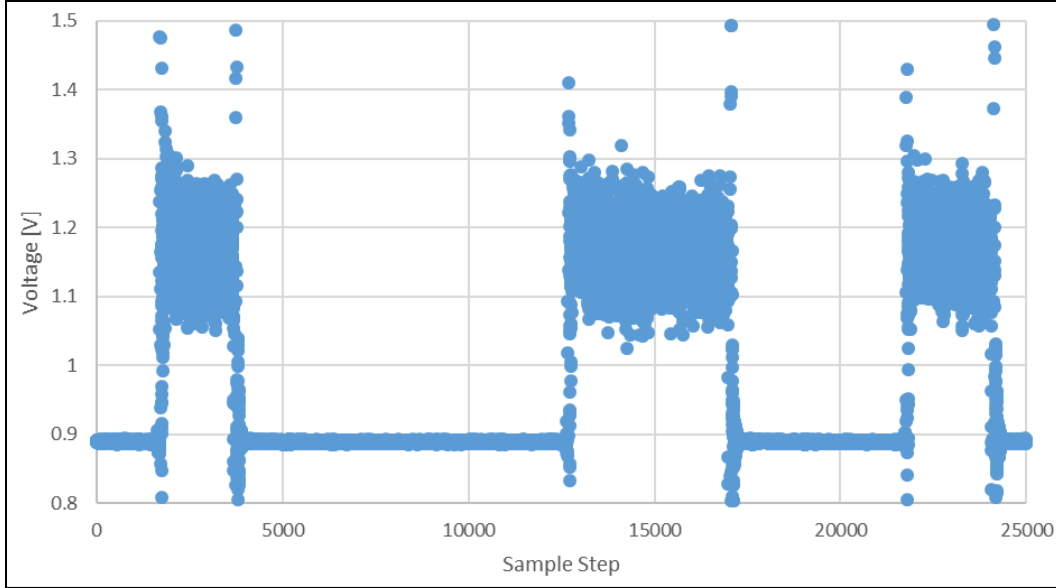


Figure 12: Voltage signal used in for the uncertainty analysis.

The last major source of error within measuring the system comes from the motion of the hose moving from one bucket to the next. The following is a proof to show it is reasonable to neglect any uncertainty that may arise due to the movement of the hose. To start, the following values are known: density of water ( $\rho_{H_2O}$ ), radius of the tube ( $r_t$ ), the distance between the two buckets ( $w$ ), radius of bucket 1 ( $r_1$ ), radius of bucket 2 ( $r_2$ ), the height of the tube above the edge of the bucket ( $h$ ), and gravity ( $g$ ). In this scenario, (A) is the volume of water, called  $V_1$ , above Bucket 1, (B) is the volume of water while moving to Bucket 2, (C) is the volume of water, called  $V_2$ , above Bucket 2, and (D) is the volume of water while moving to Bucket 1. The following assumptions are made:

- 1)  $h \rightarrow$  Constant.
- 2) System is steady-state;  $\dot{m} \rightarrow$  Constant;  $\rho \rightarrow$  Constant.
- 3) Top of the buckets is the datum line.

- 4) The movement of the tube from one bucket to the next is perfectly synchronized with the starting and stopping of the stopwatch.
- 5) The columns of water (A) and (C) are perfectly centered on the centerline of each bucket.
- 6) The tube moves horizontally back and forth with constant velocity, and zero velocity in the vertical direction.
- 7) Any  $V_i$  of water will have the same cross-sectional area as the inner diameter of the tube.

The following is the proposal of proof; if the volumes of water,  $V_1$  and  $V_2$ , are the same volume, then mass error is negligible.

From assumption (7), the volumes of water should maintain the same cross-sectional area as the inner diameter of the tube. It should be noted this is a very harsh assumption and should not be taken lightly. It is likely that the cross-sectional areas will not be the same, but the assumption is made to simplify the math. Therefore, it can be said that  $V = AL$ , where  $L$  is the length of the centerline of the volume of water, and  $A$  is the cross-sectional-area.

Since both  $V_1$  and  $V_2$  came from the same tube, they will have the same cross-sectional area at any infinitesimal point  $dL_i$ . Since each slice of  $dL$  in each volume is the same, only the length of the centerline of each column of water needs to be compared. To do this, let us use the equation for finding the length of a curve, found in any college calculus textbook,  $L = \int_a^b \sqrt{1 + (dy / dx)^2} dx$ , where  $a = x\text{-position}(r_1)$ . The distance the tip of the tube travels is the distance where the centerline of the tube moves from and to the centerline of each bucket. Calling  $a = 0$ , then  $b$  is defined as  $b = r_1 + r_2 + w$ . Since the buckets are the same size and height,  $r_1 = r_2 \rightarrow b = 2r + w$ . Thus,  $L_{A \rightarrow B} = \int_0^{2r+w} \sqrt{1 + (dy / dx)^2} dx$ . Using assumption (6), the tube moves horizontally at a constant rate, as well as assumption (2), the system is steady state, the water falls based on initial exit velocity and the force of gravity. It would be expected that the

water has some parabolic curve. Let us call this curve to be  $y = x^2 + h$ . Therefore,  $\frac{dy}{dx} = 2x$ .

For the ease of proof, let us say  $b = 2r + w = 1$ . Therefore,  $L_{A \rightarrow B} = \int_0^1 \sqrt{1 + 4x^2} dx$ . Solving this integral yields  $L_{A \rightarrow B} = 1.4789$ . Since no dimensions or properties have changed, the entire process is reversible, yielding  $L_{C \rightarrow D} = 1.4789$ .

Thus, the two columns have the same cross-sectional area and the same length of centerline. Therefore,  $V_1$  and  $V_2$  must be identical volumes. Since density is constant, the mass exchange is identical, and it is reasonable to assume that any errors cancel out. Again, this is a harsh assumption that is only made to simplify the math. A more accurate representation of this will lead to a more reasonable estimation of the uncertainty.

However, in reality, there will be errors because the listed assumptions cannot be guaranteed to always hold true. The height and velocity of the hose may vary slightly, and irregularities within the setup can introduce errors. In general, the error will depend upon the height of the tube from the buckets, human reaction time, and distance travelled in the  $x$ -direction. To demonstrate the influence from height, we look at the Bernoulli equation,

$$\frac{P_1}{\rho} + \frac{V_1^2}{2} + gz_1 = \frac{P_2}{\rho} + \frac{V_2^2}{2} + gz_2. \quad (3.18)$$

The following assumptions are made:

- 1)  $z_1 - z_2 = h$ , where  $z_1$  is the point just past the exit of the tube,  $z_2$  is the top edge of the bucket, and  $h$  is the difference between them.
- 2)  $P_2 = 0$  (gauge), where  $P_2$  is the pressure at point 2.
- 3)  $P_1 = 0$  (gauge), where  $P_1$  is the pressure at point 1.

Thus, the Bernoulli equation reduces to  $2gh = V_2^2 - V_1^2 \rightarrow V_2^2 = 2gh + V_1^2$ . This makes sense because as the distance between the tube and the top of the buckets increases, the water falls

farther, accelerating with gravity. Height plays another role, along-side human reaction time. This can be demonstrated by looking at Reynolds Transport Theory applied for the conservation of mass,

$$\frac{dm_{sys}}{dt} = \frac{\partial}{\partial t} \int_{CV} \rho dV + \int_{CS} \rho V \cdot \hat{n} dA = 0. \quad (3.19)$$

This system of equations is dependent upon time, and because of error in human reaction time, there will be an inherent advance or lag. When going from A→B, any advance in time will result in an increased measure of mass (overestimate) and any lag will result in a decreased measure (underestimate). When going from C→D, the opposite is true. Due to human reaction time not being perfect, there will always be an error. There are only 2 obvious exceptions to this:

- 1) When an advance in A→B is equal to an advance in C→D.
- 2) When a lag in A→B is equal to a lag in C→D.

In these two cases, any errors will cancel out, assuming they are identical.

Lastly, in regards to tube motion, the position of the tube relative to the centerline of each bucket introduces error by directly affecting the distance travelled, resulting in a similar outcome to the advance or lag due to time previously discussed. However, this error is minimal compared to human reaction time and the dependency on the height of the tube. Furthermore, it cannot be directly measured with the current setup. In order to simplify matters, the height of the tube can be held roughly constant. Overall, this leads to human reaction time being the primary source of error in this case, both in moving to and moving from the collection bucket. Therefore, the uncertainty of mass measurement can be very roughly estimated as 2x human reaction time, in addition to the CPWplus-35 uncertainty because it cannot be guaranteed that the collection of mass is perfectly synchronized with the starting and stopping of the stopwatch,

$$\epsilon_{\dot{m}_i} = \dot{m}_i \sqrt{\left(\frac{\epsilon_m}{m_i}\right)^2 + 2 * \left(\frac{\epsilon_t}{t_i}\right)^2}. \quad (3.20)$$

Next, the pressure drop is calculated as  $\Delta P = m_{calibrated} * \Delta V$ , where  $m_{calibrated}$  is a calibration factor obtained while calibrating the PT. Based on the rules for propagation of uncertainty, the uncertainty for the pressure drop will be

$$\epsilon_{\Delta P_i} = \Delta P_i \sqrt{\left(\frac{\epsilon_m}{m_i}\right)^2 + \left(\frac{\epsilon_{\Delta V}}{\Delta V_i}\right)^2}. \quad (3.21)$$

The next important property is the Reynolds Number, which is defined as

$$Re = \frac{dU}{\nu}. \quad (3.22)$$

Here the average pipe velocity  $U$  is calculated as  $U = m/t\rho A$ . Therefore, neglecting uncertainty with pipe area as explained above, the uncertainty of the local velocity is defined as

$$\epsilon_{U,i} = U_i \sqrt{\left(\frac{\epsilon_m}{m_i}\right)^2 + \left(\frac{\epsilon_t}{t_i}\right)^2 + \left(\frac{\epsilon_\rho}{\rho_i}\right)^2}. \quad (3.23)$$

From this, the uncertainty when calculating the Reynolds Number, neglecting uncertainty with pipe diameter, is

$$\epsilon_{Re_i} = Re_i \sqrt{\left(\frac{\epsilon_U}{U_i}\right)^2 + \left(\frac{\epsilon_\nu}{\nu}\right)^2}. \quad (3.24)$$

Next the Fanning friction factor is calculated from the pressure drop measurement following the analysis described above,

$$f = \frac{d}{2U^2} \frac{\Delta P}{\Delta x}, \quad (3.25)$$

Based on the explanation for square of uncertainty provided by Harvey (2016) regarding  $U^2$ , the uncertainty for the Fanning friction factor, neglecting pipe diameter uncertainty, takes the form of

$$\epsilon_{f_i} = f_i \sqrt{\left(2 * \frac{\epsilon_{U_i}}{U_i}\right)^2 + \left(\frac{\epsilon_{\Delta P_i}}{\Delta P_i}\right)^2} + \epsilon_{\Delta x}^2. \quad (3.26)$$

Using these values, the data is plotted in a PK plot as  $Re f^{0.5}$  vs.  $f^{-0.5}$ . To plot the abscissa (i.e.  $x$ -coordinate) of this, the uncertainty can be represented as

$$\epsilon_{Re f^{0.5}} = (Re f^{0.5})_i \sqrt{\left(\frac{\epsilon_{Re_i}}{Re_i}\right)^2 + \left(0.5 \frac{\epsilon_{f_i}}{f_i}\right)^2}. \quad (3.27)$$

Similarly, the uncertainty of the ordinate ( $y$ -coordinate) will take the form of

$$\epsilon_{f_i}^{-0.5} = f_i^{-0.5} \left(\frac{\epsilon_{f_i}}{f_i}\right). \quad (3.28)$$

Both the Reynolds number and the Fanning friction factor have varying uncertainty for each data point acquired. As such, it is easier to represent the uncertainty in the experimental measurements using error bars. Figure 13 and Figure 14 demonstrate this uncertainty representation, with the black, vertical error bars representing  $f^{0.5}$  and the red, horizontal error bars representing  $Re f^{0.5}$ . It is clear from this plots that, for increasing values of  $Re$  and  $f$ , the relative uncertainty decreases. The dashed line in each figure represents the fitted equation based on the concentration.

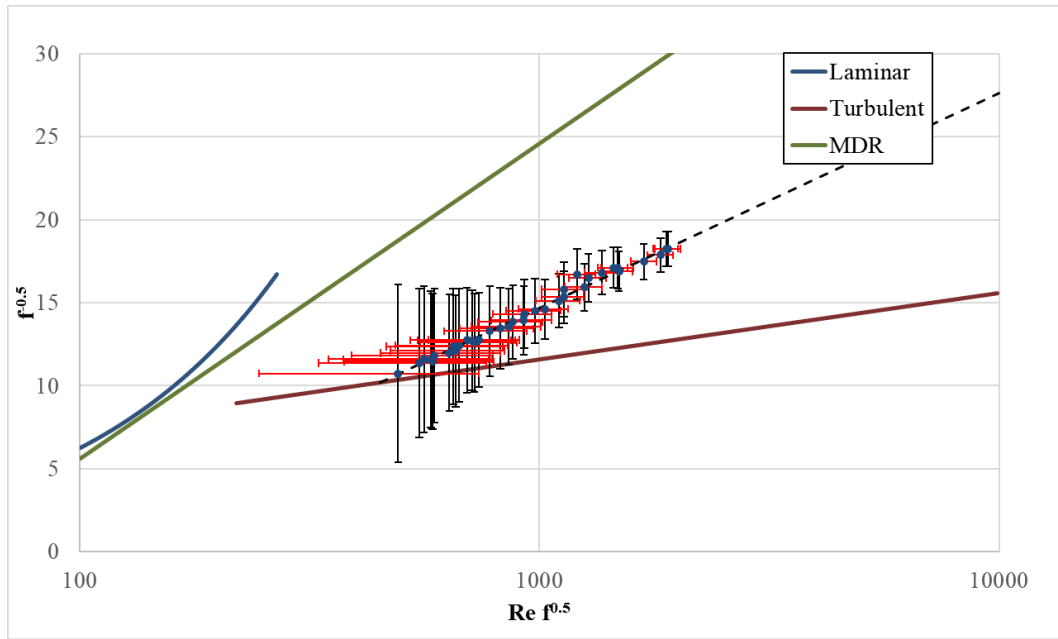


Figure 13: Representation of drag reduction uncertainty using error bars. Concentration 15 ppm.

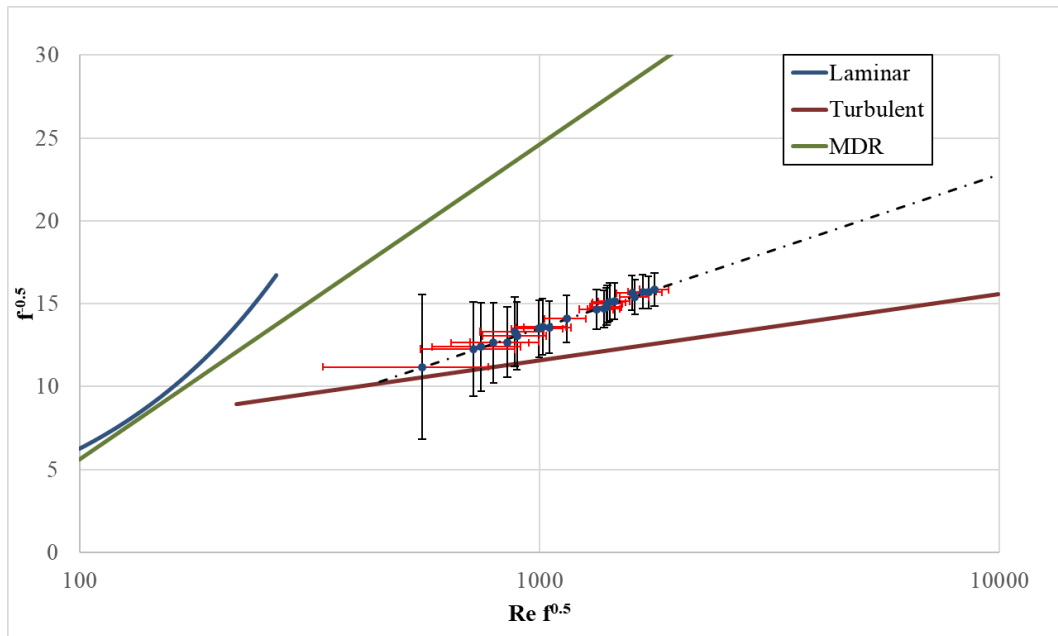


Figure 14: Representation of drag reduction uncertainty using error bars. Concentration 10 ppm.

After all data points have been plotted, they are fitted with a least-squares line fit method. Therefore, it is necessary to determine the uncertainty of the line fit. Using the tool named Data Analysis ToolPak, included with Excel, to perform linear regression, an estimate of the standard

error of the slope and the intercept can be made. Using all the above equations, the uncertainty of  $M_w$  can be estimated. Molecular weight is defined based on the shear rate of the onset of drag reduction ( $\gamma^*$ ) as given in equation (3.1). Rearranging this, plugging in definitions for  $U$  and  $f$ ,  $M_w$  can be solved as

$$M_w = \frac{2 * 3.35 \times 10^9}{\frac{1}{2} \frac{\left(\frac{Re * \nu}{d}\right)^2 \left(1/f^{-0.5}\right)^2}{\nu}}, \quad (3.29)$$

where the following is true at the onset of drag reduction becomes

$$Re * f^{0.5} = e^{\frac{B_{H_2O} - B_{poly}}{A_{poly} - A_{H_2O}}}. \quad (3.30)$$

As previously mentioned,  $B_{H_2O} = -0.4$  and  $A_{H_2O} = 1.737$ . Simplifying this expression results in

$$M_w = \frac{d^2}{\nu} \frac{6.7 \times 10^9}{\left(e^{\frac{-0.4 - B_{poly}}{A_{poly} + 13.906}}\right)^2}, \quad (3.31)$$

which allows the calculation of  $M_w$ . Based on this, using the rules of propagation of uncertainty according to Harvey (2016), neglecting the uncertainty of pipe diameter and holding  $\nu$  constant for water, the estimation for the uncertainty of  $M_w$  can be found.

### 3.1.7 Results

When looking at the drag reduction capabilities of the polymer solutions, the point where drag reduction begins is almost exclusively independent of the solution concentration (Virk, 1975). This point where drag reduction begins is referred to as the onset of drag reduction. Furthermore, all solutions that have no degradation should register the same  $M_w$  when using the

formulation described above. According to the DOW Chemical Company, WSR-301 should have a molecular weight of approximately  $4 \times 10^6$  g/mol.

In Figure 15, two concentrations were prepared multiple times using the method prescribed in this paper. The onset of drag reduction for a concentration of 15 ppm occurs at  $Re = 452$ , and the onset of drag reduction for a concentration of 10 ppm occurs at  $Re = 435$ . The calculated molecular weight of each of the trials with a concentration of 15 ppm ranged from 3.70 to 4.39, with an average of 4.02. The calculated molecular weight of each of the concentration of 10 ppm trials ranged from 3.94 to 4.49, with an average of 4.11. The overall error between all trials and the actual estimate of the molecular weight ranged from 0.34% to 12.13%, with an average error of 4.34%. Table 7 gives an overview of the variations in molecular weight for each concentration. The set of data points following the Turbulent line are the water calibration data sets, taken before each data acquisition.

These molecular weight values are in good agreement with the estimated molecular weight of WSR-301 described by the DOW Chemical Company. Additionally, based on the explanations of Harvey (2016), the calculations of the uncertainty of the Mw of WSR-301 using a comparison against water is estimated and tabulated near the bottom of Table 7.

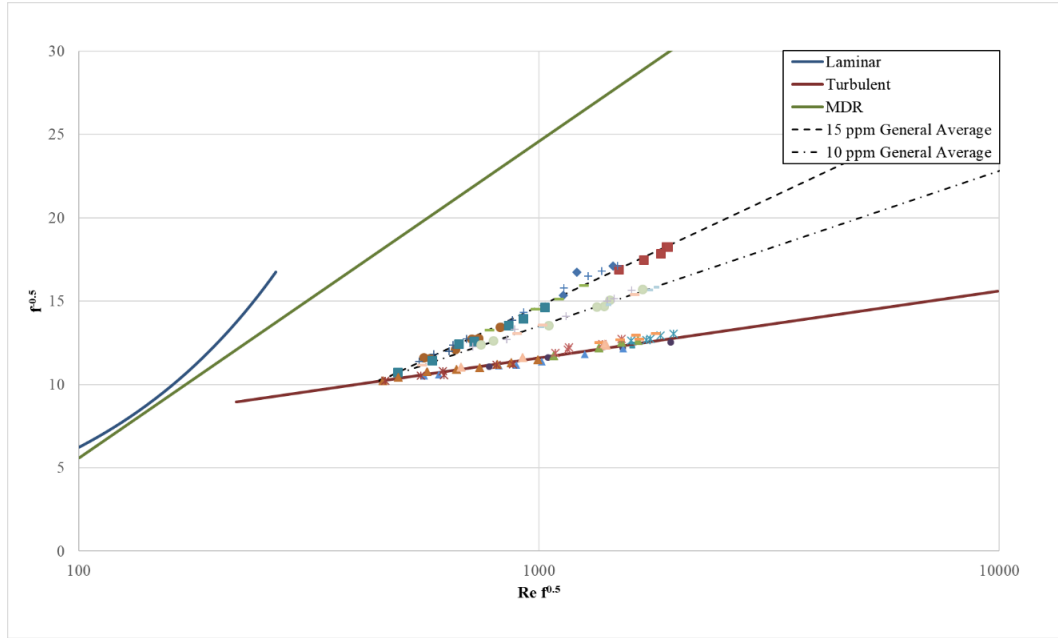


Figure 15: The above figure shows how the drag reduction profiles of the polymer solutions vary based on concentration.

Table 7: General summary of molecular weight estimations. Error calculations are based on the estimated molecular weight of WSR-301 ( $M_w \times 10^6 = 4.0$ ) provided by the DOW Chemical Company.

		15	10	Overall
<b>Mw</b> $\times 10^{-6}$ (g/mol)	<b>Min</b>	3.70	3.94	3.70
	<b>Max</b>	4.39	4.49	4.49
	<b>Mean</b>	4.02	4.11	4.06
<b>Error (%)</b>	<b>Min</b>	0.34%	0.95%	0.34%
	<b>Max</b>	9.85%	12.13%	12.13%
	<b>Mean</b>	4.47%	4.11%	4.34%
<b>Uncertainty of Mw (g/mol)</b>	<b>Min</b>	3.25	3.44	
	<b>Max</b>	4.75	4.56	
<b>Onset DR Re</b>		452	435	444

This is in good agreement with our experimental results. Furthermore, the Onset Drag Reduction Reynolds numbers are within 4% of each other. This agrees with Virk's (1975) observation that the Onset DR Reynolds number remains mostly unchanged as the concentration of the solution changes.

Additionally, in Figure 15, there are two dashed lines, each representing a line of best fit found using linear regression. The equation for the 15 ppm line is

$$f^{-0.5} = 5.619 \ln(Re f^{0.5}) - 24.138, \quad (3.32)$$

and the equation for the 10 ppm line is

$$f^{-0.5} = 4.0379 \ln(Re f^{0.5}) - 14.379. \quad (3.33)$$

Table 8 shows the calculated values estimating uncertainty. The time uncertainty is 0.142 seconds,  $\Delta x$  uncertainty is 0.076 m, temperature uncertainty is 0.5°F, uncertainty of mass measurement with the CPWplus-35 scale is 0.0141 kg, and the uncertainty with the Cole-Parmer scale is 0.0329 g. Table 9 shows the calculated uncertainty of the voltages,  $V_0$  and  $V_{\text{Measure}}$ , which are 1.29 mV and 38.9 mV respectively. Figure 13 and Figure 14 visually demonstrate the error associated with each point of the Virk Tube analysis. Appendix C provides tabulated data for this analysis.

*Table 8: Uncertainty estimations for Time,  $\Delta x$ , mass measurement of the CPWplus-35 scale, the Cole-Parmer scale, and temperature measurement.*

Time (s)		$\Delta x$ (m)		Mass (g) Cole-Parmer	
<b>Target</b>	10	<b>Target</b>	1.05	<b>Resolution</b>	0.01
<b>Average</b>	10.052	<b>C</b>	0.540	<b><math>\Delta</math> Avg</b>	-2.97E-02
<b>Std.Dev.</b>	0.131	<b>Resolution</b>	0.03	<b>Std. Dev.</b>	3.06E-02
<b>Resolution</b>	0.01	<b>Hole Accuracy</b>	0.0625	<b><math>\Delta m</math> Avg</b>	6.67E-03
<b>Uncertainty (<math>\epsilon_t</math>)</b>	0.142	<b>Uncertainty (<math>\epsilon_{\Delta x}</math>)</b>	0.076	<b>Uncertainty (<math>\epsilon_{mCP}</math>)</b>	3.29E-02
Mass (kg) CPWplus-35		Temperature (°F)			
<b>Resolution</b>	0.01	<b>Resolution</b>	1		
<b><math>\Delta m_{1-2}</math></b>	0.01	<b>Read</b>	0.50		
<b>Uncertainty (<math>\epsilon_{m35}</math>)</b>	1.41E-02	<b>Uncertainty (<math>\epsilon_{temp}</math>)</b>	0.5		

Table 9: Uncertainty estimations for  $V_0$ ,  $V_{measure}$ , and  $\Delta V$ .

$V_0$ (V)		$V_{Measure}$ (V)		Voltages (V)	
Std. Dev.	1.29E-03	Std. Dev.	3.89E-02	Resolution	1.00E-06
$\Delta V_0$	-9.06E-05	$\Delta V_{Measure}$	3.43E-03	$\Delta V$	
Uncertainty ( $\epsilon_{VZero}$ )	1.29E-03	Uncertainty ( $\epsilon_{VMeasure}$ )	3.89E-02	Uncertainty ( $\epsilon_{\Delta V}$ )	3.90E-02

## 3.2 Apparent viscosity

### 3.2.1 Rheometer

Rheological analysis was performed on the polymer solutions with a cone-and-plate rheometer (Discovery Hybrid Rheometer-2, TA Instruments, New Castle, DE, USA). The cone fixture on the spindle-rod was a 60 mm diameter with a 2° 36" cone angle. Unfortunately, the Peltier plate (i.e. flat plate) on the rheometer was damaged by the previous users that caused errors in the temporal response of the rheometer. However, the mean viscosity at a given shear rate was shown to match results using an identical rheometer. A minimum polymer concentration of ~50 ppm is required to accurately measure the viscosity. The software used to control the rheometer and record data is TRIOS (Version 4.3.0, TA Instruments, New Castle, DE, USA).

### 3.2.2 Test procedures

A new set of samples was prepared for the viscometer testing. Unlike in the molecular weight testing, a new sample with a concentration of  $C = 1000\text{ppm}$  was made. Testing procedures are based on the help files provided by TA Instruments (2013). To begin, with the power to the system turned off, the air supply to the rheometer is turned on, and the pressure required for the system, is 30 psi. The bearing lock on the rheometer is removed, and the spindle is checked to spin without obstruction. If the spindle spins without obstruction, then the rheometer is powered

on. Additionally, the water supply to the Peltier plate is turned on. If no alarms on the rheometer begin to sound, then the TRIOS software is loaded.

Each spindle rod is equipped with a band, located near the edge where it attaches to the rheometer. This band allows for what is known as “smart swap”, which allows the rheometer to automatically read and load all necessary data and geometry about the rod. Though this process is automatic, it is encouraged to double-check what the rheometer reads. Afterwards, a small sample (in this case, about 2 mL) of polymer solution is taken and placed in the rheometer. The height of the rod is adjusted until it reaches an appropriate gap height, based on the geometry of the rod.

### 3.2.3 Data analysis and model fitting

When working with macromolecular fluids, it is important to be capable of accurately predicting various properties. A model is useful for an estimation of viscosity beyond what might be capable with available tools. Since PEO, like many polymer solutions, is a shear thinning fluid, it can be fit using the Carreau-Yada model,

$$\frac{\mu - \mu_{\infty}}{\mu_0 - \mu_{\infty}} = [1 + (\lambda\dot{\gamma})^a]^{\frac{n-1}{a}}. \quad (3.34)$$

For many polymer solutions, including PEO, the Carreau-Yada model can be reduced to

$$\mu = \mu_0 [1 + (\lambda\dot{\gamma})^2]^{\frac{n-1}{2}}. \quad (3.35)$$

When applying the Carreau model, plotted as the dashed line in Figure 16 and Figure 17, to the rheometer data contained within this thesis, the following parameters were chosen:  $n = 0.89$ ,  $\lambda = 0.27$  s, and  $\eta_0 = 0.0055$ . This model appears to agree well with the rheometer data, but appears to be diverging slightly from the experimental data at about  $\dot{\gamma} = 300$  s<sup>-1</sup>. Note that the deviation from the model at shear rates above  $\sim 300$  s<sup>-1</sup> is an established inertioelastic instability (Larson, 1992),

which comparison of the apparent viscosity should be applied prior to this instability (Elbing et al., 2011). Additionally, the deviations at low shear rates are associated with the limit of the rheometer.

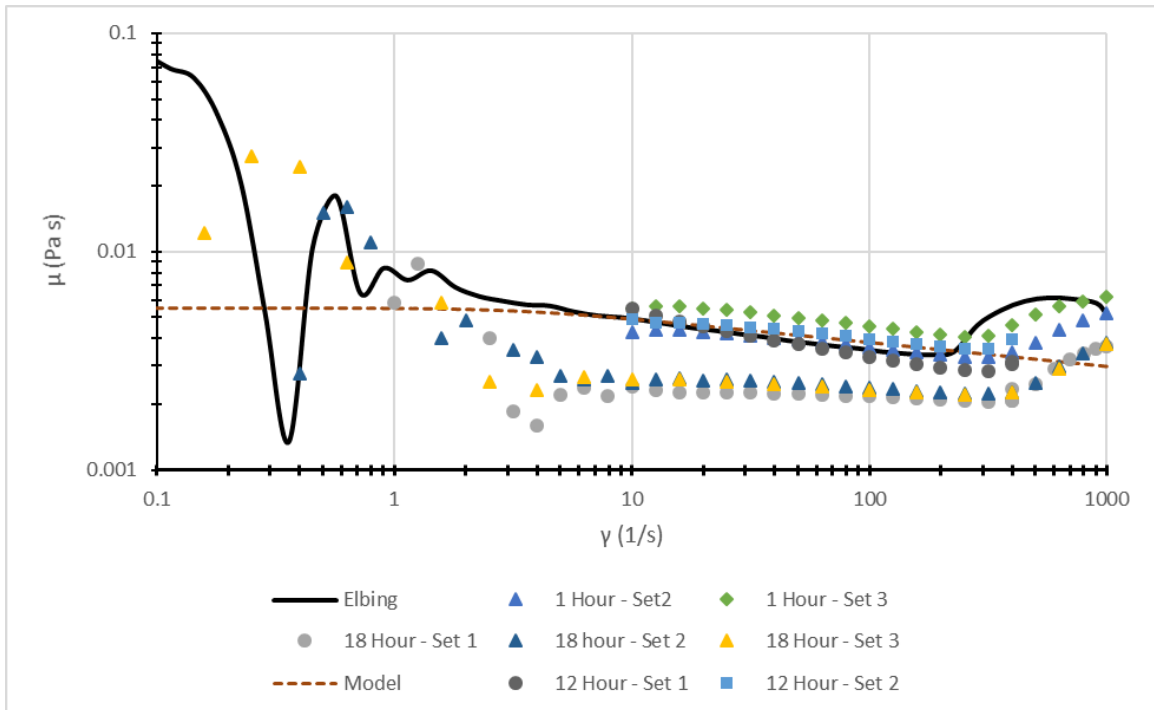


Figure 16: A Comparison of the viscous properties of WSR-301, concentration 1000 ppm, according to the time between preparation and testing.

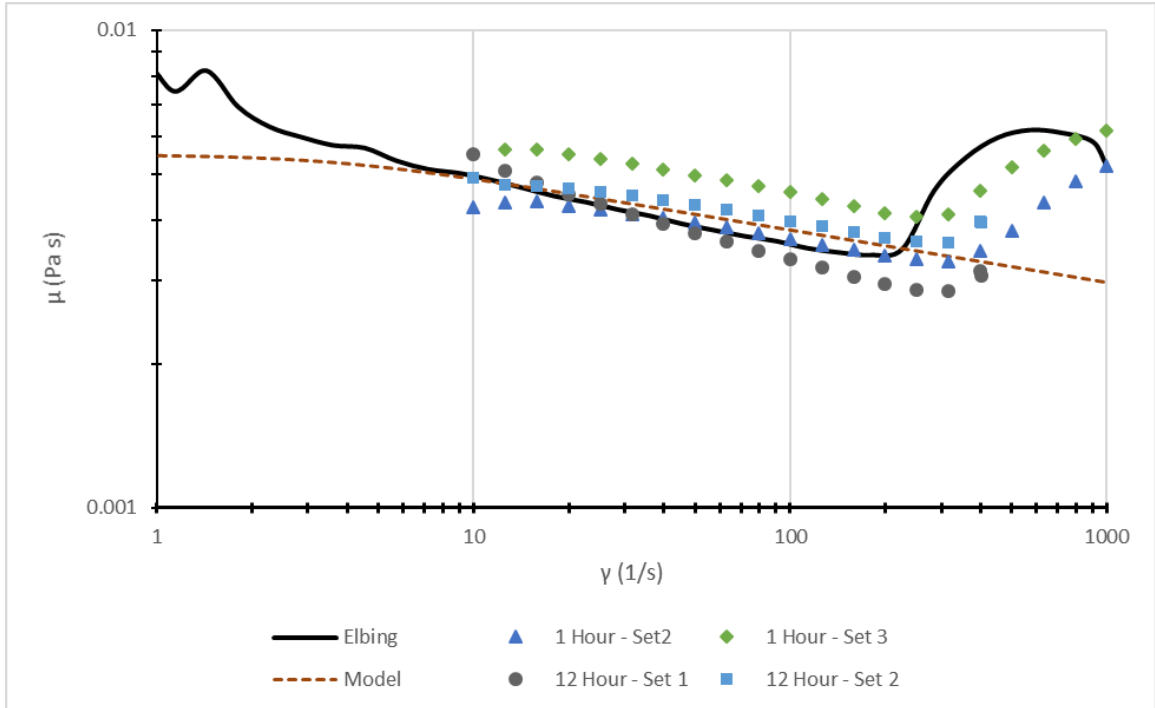


Figure 17: A zoomed in version of Figure 16.

### 3.2.4 Uncertainty analysis

Due to the proprietary nature of the DHR-2, it is difficult to analyze individual contributors to the uncertainty. Thus, to estimate the uncertainty of the rheometer, the repeatability of the data sets will be examined. Table 10 shows the standard deviation of each dataset, based on the viscosity readings of each sample. The maximum standard deviation is very low for each of the 1 hour, 12 hour, and 18 hour samples. From this, it is apparent that the testing procedures for the rheometer produce repeatable results with a very low difference between measurements individual measurements. However, when plotting the 18 hour data, even though all cases were consistent, it was obviously degraded compared to the other samples. For this reason, it will not be considered for any results other than repeatability of sampling.

Table 10: Standard deviation data of viscosity datasets for 1, 12, and 18 hour samples

Set	Min $\sigma$	Max $\sigma$	Avg $\sigma$
1 Hour	5.32E-04	9.61E-04	7.46E-04
12 Hour	5.57E-05	6.39E-04	4.00E-04
18 Hour	5.23E-05	2.00E-04	1.23E-04

There is an issue worth noting about the rheometer used for gathering this data. First, the Peltier plate used with this rheometer is damaged. It has a small bump on the surface, and it is very likely this will affect any data gathered with this system. During the data acquisition, there was a tendency for measurements to exhibit a sinusoidal pattern of measurement. In order to counteract this observation, data points were recorded for a longer amount of time to average out the sinusoidal behavior. As previously mentioned, this approach matched well with results from an identical rheometer that was not damaged.

### 3.3 Relaxation time

#### 3.3.1 Intrinsic viscosity

The relaxation time for a polymer, in the most basic sense, is the maximum amount of time needed for all the elastic polymer structures in a solution to relax after being stretched. However, it is difficult to produce accurate results for this value, especially at high molecular weights and high concentrations. Consequently, for the PEO solutions of interest empirical relationships are required, but the behaviors are different depending on whether the solutions is dilute. Intrinsic viscosity is required to estimate the overlap concentration, which is the boundary between dilute and non-dilute solutions. The Mark-Houwink relationship with constants determined for PEO solutions (Bailey & Callard, 1959),

$$[\eta]_o = 0.0125M_w^{0.78}, \quad (3.36)$$

establishes a relationship between the molecular weight and the intrinsic viscosity. Here  $M_w$  is the molecular weight and  $[\eta]_o$  is the intrinsic viscosity. The overlap concentration, which is concentration when molecules begin to have significant interaction with molecules, is readily obtained from the intrinsic viscosity,

$$C^* = 1/[\eta]_o. \quad (3.37)$$

From equation (3.36), based on the estimated  $M_w$  for WSR-301 from the DOW Chemical Company, the intrinsic viscosity should be  $[\eta]_o = 1764.07 \text{ cm}^3/\text{g}$  and consequently has an overlap concentration of  $C^* = 567 \text{ ppm}$ . Note that in practice the mean molecular weight obtained from the Virk tube is used to determine the given batches corresponding intrinsic viscosity and overlap concentration. Given the overlap concentration, the relaxation time can be estimated from the Zimm time and Kalashnikov time if the sample is dilute or non-dilute, respectively.

### 3.3.2 Zimm time

Zimm time is a measure of the relaxation time for polymer solutions with high molecular weights at low concentrations, and it applies below the overlap concentration. The Zimm relaxation time is defined as

$$\lambda_z = 0.422 \frac{[\eta]_o \mu_s}{RT} M_w, \quad (3.38)$$

where  $T$  is the absolute temperature,  $R$  is the ideal gas constant,  $[\eta]_o$  is the intrinsic viscosity, and  $M_w$  is the molecular weight.

### 3.3.3 Kalashnikov time

In contrast to the Zimm time, Kalashnikov time (Kalashnikov, 1998) is a measure of the relaxation time for high molecular weight polymer solution with very high concentrations above the overlap concentration, and it is defined as

$$\lambda_k = \left[ \frac{[\eta]_o}{549.5} - \left( \frac{[\eta]_o}{3255} \right)^3 - 0.51 \right] \exp\{-(T_c/50)^2\} C^{0.5}, \quad (3.39)$$

where  $C$  is the concentration of the solution,  $[\eta]_o$  is the intrinsic viscosity, and  $T_c$  is the temperature in degrees Celcius.

### 3.3.4 Results

For WSR-301, Table 11 below lists the testing parameters used and the resulting relaxation time values. These values agree well with Winkel et al. (2009).

Table 11: Testing parameters for viscosity testing and resulting relaxation time values.

Testing Parameters			
$\mu_s$ [m <sup>2</sup> /s]	1.0533E-06	Temp [°C]	20
$M_w$ [g/mol]	4000000	C [ppm]	1000
	R [N*m/kmol*K]	8.314	
Relaxation Time Values			
$[\eta]_o$ [cm <sup>3</sup> /g]	1764.07	$\lambda_z$ [ms]	1.29
C* [ppm]	566.87	$\lambda_k$ [s]	2.17
	$\Delta/c$ [1/ppm]	808.85	

### 3.4 Polymer parameter calculations

#### 3.4.1 Weissenberg number

The Weissenberg number ( $Wi$ ) is a dimensionless number relating the rheological reaction time of the viscous forces to the elastic forces of the fluid, and it is determined by comparing the characteristic time (the relaxation time) of the working fluid (in this case, Kalashnikov time,  $\lambda_k$ ) to the rate of deformation (McKinley, 2005), shown in equation (3.40). Thus, it is expected that for any fluid, there will be a range of  $Wi$  for any single fluid. What makes the determination of  $Wi$  difficult is selecting an appropriate relaxation time. Polymer solutions can have a range of relaxation times that govern the nonlinear rheological characteristics of the flow (Slattery, 1968). However, since the concentration of the samples, 1000 ppm, exceeds the overlap concentration of 566 ppm, the method developed by Kalashnikov (1998) for determining relaxation time for dilute polymer solutions makes it possible to calculate the Weissenberg. This range of  $Wi$  is plotted in Figure 18.

$$Wi = \frac{\lambda U_\infty}{\delta} = \dot{\gamma} \lambda \quad (3.40)$$

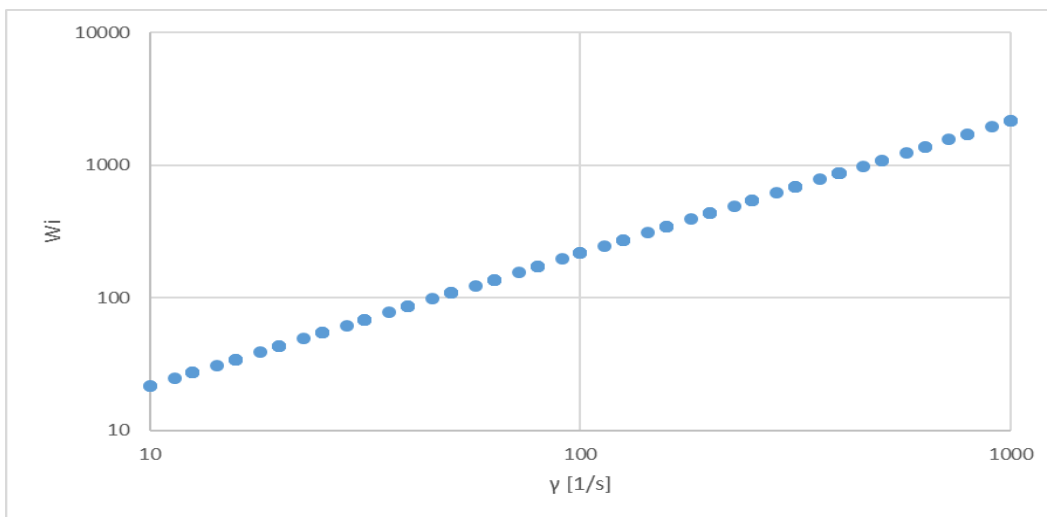


Figure 18: Weissenberg number vs shearing rate

### 3.4.2 Viscosity ratio ( $\mu^*$ )

The viscosity ratio,  $\mu^*$ , is the ratio of the solvent viscosity,  $\mu_s$ , to the zero-shear viscosity of the polymer solution,  $\mu_o$  (Kalashnikov, 1993; 1998). As the Mw of the polymer in question increases, the difference in limiting viscosities,  $\Delta$ , will also increase,

$$\Delta \equiv \frac{\mu_o - \mu_\infty}{\mu_\infty} = \left[ \left( \frac{[\eta]_o}{135.6} \right)^2 + 0.434[\eta]_o - 126 \right] C. \quad (3.41)$$

From this relationship, the viscosity ratio for PEO at concentration of 1000 ppm is  $\mu^*=1.24E-6$ .

### 3.4.3 Length ratio

The length ratio, L, describes the ratio of the fully extended polymer chain length to the fully-coiled length. The fully stretched length is directly proportional to the Mw of the polymer in question, according to Larson (1999), defined as

$$L_{ext} = \frac{0.82l_o n_o M_w}{M_o}. \quad (3.42)$$

Here  $n_o$  is the number of backbone bonds in each monomer of the molecule ( $n_o = 3$  in the case of PEO).  $M_o$  is the molar mass, and  $l_o$  is the average length of each backbone bond. The fully coiled length is difficult to know exactly, but typically is estimated using a series of random walks. Due to the nature of Brownian motion, the molecules in the solution remain isotropic, and when working with extremely long chains, such as WSR-301, a time-averaged mean-square distance can estimate the random-walk as  $\langle R^2 \rangle_0 = n_o b_n^2$ , where  $b_n$  is the length of an average walk.

Using these definitions, the coiled length can be approximated as  $L_{coil} = 0.82l_o n_o (M_w/M_o)^{0.5}$ .

When combining these properties together, the length ratio comes out to be dependent on the

molecular weights. In this case,  $M_o = 44.1$  g/mol and  $M_w = 4000000$  g/mol. The resulting length ratio

$$L = \left(\frac{M_w}{M_o}\right)^{0.5}, \quad (3.43)$$

comes out to  $L = 301$ .

## CHAPTER IV

### CASE STUDY: SYRINGE PUMP DEGRADATION

#### ***4.1 Syringe pump description***

The syringe pump (shown in Figure 19) is a custom designed, low-flow rate injector (Bonk et al., 2017), designed and built at Oklahoma State University. It is powered by a non-captive, NEMA 34 linear stepper motor with an 18” lead screw, which is attached to an aluminum rod. This aluminum rod depresses and retracts 4 plungers to expel polymer or other solutions, contained within the syringe tubes, through a custom injector plate. Each syringe tube is acrylic, 15” in length with a 2.5” ID. The entire system was built and calibrated to have a maximum injection rate of 0.104 L/s. A Raspberry Pi 3 Model B running Linux (Raspbian distro) uses a deployable python environment, from which the entire syringe pump system is controlled through a GUI and a series of scripts.

The Raspberry Pi interfaces with a MBC12101 stepper driver to control the motor. It has a current range of 1.5-10 Amps with a voltage range of 20-80V. To power the system, an unregulated open-frame external power supply was used (PSA40V4A-1). However, part of the controls for the syringe pump needed a redesign.

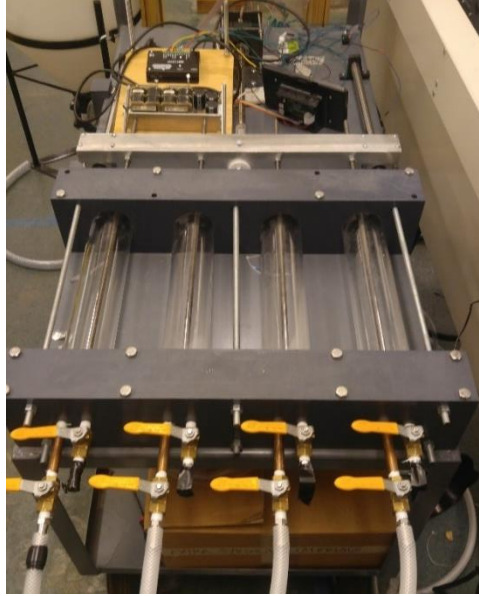


*Figure 19. Picture of the syringe pump designed and built by Bonk et al. (2017).*

The Raspberry Pi was not able to sustain a speed control signal longer than 35 seconds, and it could not produce a PWM signal capable of achieving the desired flow rates. In lieu of the Raspberry Pi, a function a DDS sweep function generator (4040B, BK Precision, Yorba Linda, CA, USA) was used to issue an imitation of the PWM signal created by the Pi. The function generator has a maximum bandwidth of 20 MHz, a peak-to-peak voltage range of 0V-10V across a 50 $\Omega$  connection, and a maximum DC offset of  $\pm 4.99$ V. It was calibrated to produce a square wave with an amplitude of 1.6V with a DC offset of 0.8V. By controlling the frequency of modulation, the speed of the motor could be tuned. This was used in tandem with the Raspberry Pi acting as an on/off and directional controller, while the function generator acted as a speed controller. A general wiring diagram is shown in *Figure 20*.

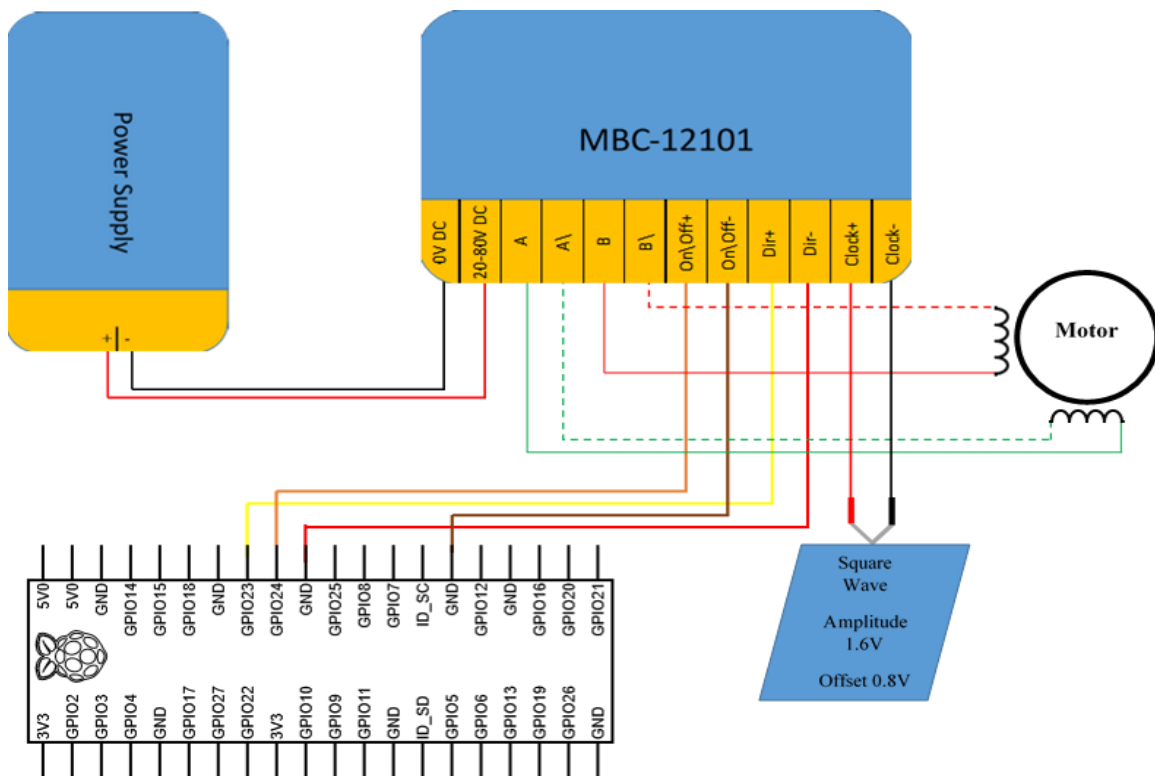


Figure 20: New wiring setup for the syringe pump. The dashed red line represents this red/white wire, and the dashed green line represents the green/white wire.

Using the ProCoach stopwatch and the CPWplus-35 floor scale mentioned earlier in this paper, the frequency of the motor was calibrated according to the mass flow rate of the system. A camera was used to record both displays at a high framerate, and this recording was played back at a slow rate. This allowed a comparison of change in mass versus change in time, resulting in mass flow rate. Figure 21 shows the real time measured data of the system. The calculated mass flow rate is plotted against actual time to show how the mass flow rate of the system is not entirely constant. Thus, an average mass flow rate is taken to represent each frequency. A total of 300 individual measurements across 5 frequencies were taken to acquire these averages. These averages were plotted and a line of best fit applied to retrieve the calibration equation (4.1),

$$\dot{m} = 1.408 * 10^{-5} f, \tag{4.1}$$

for mass flow rate vs frequency. Since higher frequencies run faster than lower, higher frequencies were repeated multiple times.

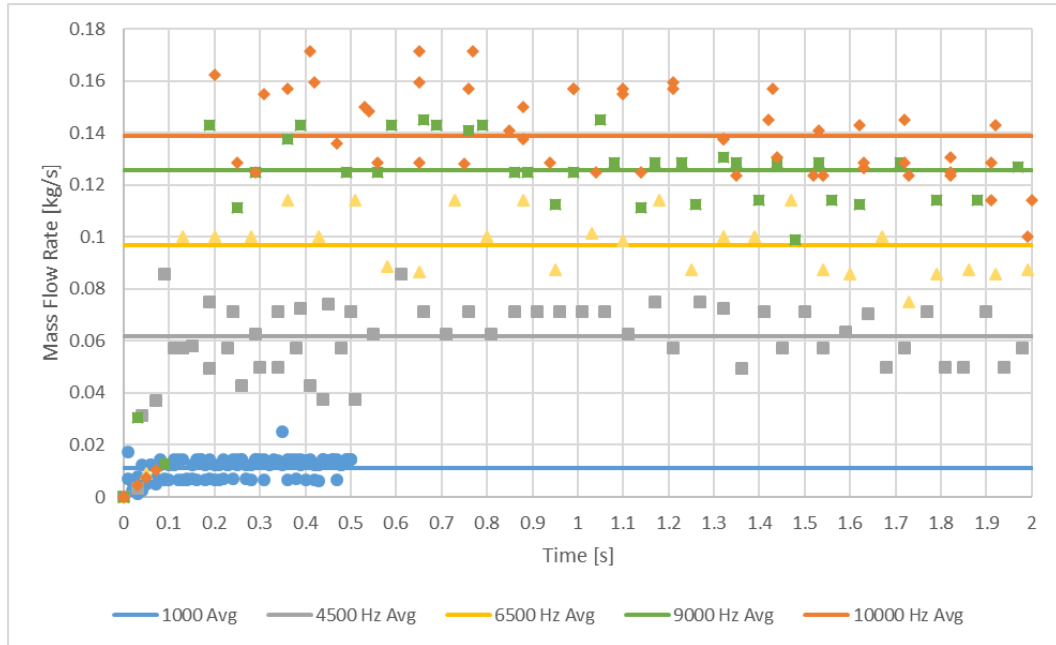


Figure 21: Instantaneous mass measurements varying with frequency.

Additionally, as the frequency climbs higher, the standard deviation of the mass flow rate grows.

Figure 22 shows the calibration curve alongside the value of the curve  $\pm 1 \sigma$ . The values used to fit these additional curves are given in Table 12.

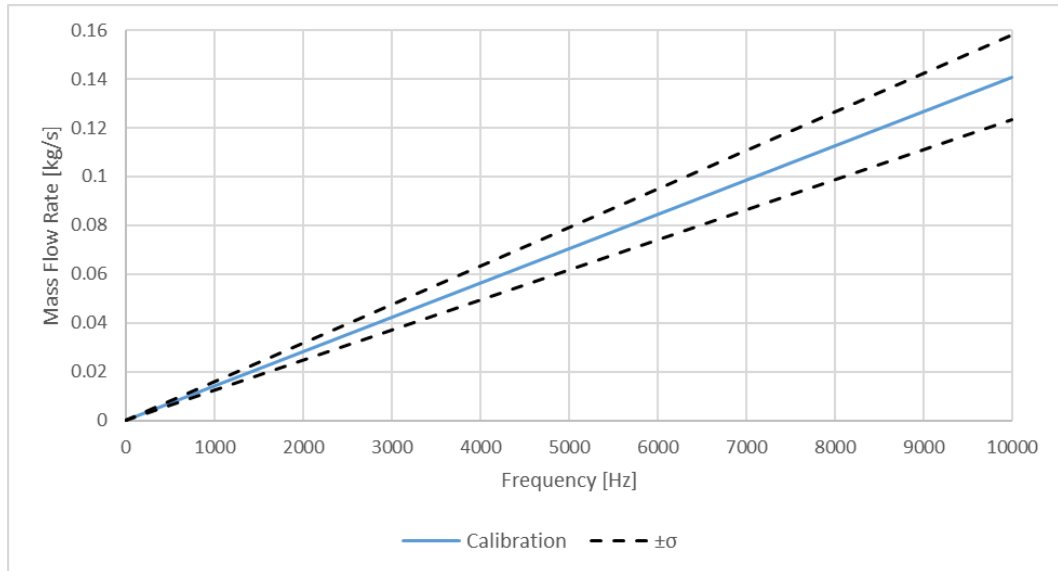


Figure 22: Mass flow rate calibrated against frequency, plotted with the change in standard deviation, which also varies with frequency.

Table 12: Calculated values and basic statistics of the mass flow rate calibration.

f [Hz]	Mdot [kg/s]	- $\sigma$ [kg/s]	+ $\sigma$ [kg/s]
0	0	0	0
1000	1.13E-02	7.31E-03	1.52E-02
4500	6.16E-02	4.92E-02	7.41E-02
6500	9.70E-02	8.56E-02	1.08E-01
9000	1.26E-01	1.13E-01	1.39E-01
10000	1.39E-01	1.22E-01	1.56E-01

## 4.2 Experimental procedure

A 1000 ppm master solution was created. Starting with the syringe pump fully plunged, the system was dialed to a frequency of 2000 Hz to begin suctioning in PEO solution from the master solution. Once the system was fully drawn, the tubes would be transferred over to an empty bucket with a scale, a stopwatch, and a camera, similar to the setup used to gather calibration data. The system was dialed to a specific frequency, based on a user-desired mass flow rate. The frequencies tested were 2000, 3600, 8000, and 9300 Hz, corresponding to 2.82E-2 kg/s, 5.06E-2 kg/s, 0.112 kg/s, and 0.131 kg/s respectively.

The system was fully-plunged, exhausting all PEO solution into the bucket. Afterwards, the solution was transferred over to the Virk tube setup, and a dilute solution of 15 ppm was made from the plunged solution. This dilute solution was tested and compared to existing drag reduction data gathered earlier in this report. This was repeated for each frequency to see at what mass flow rate the system begins to degrade the PEO solution. After each sample is plunged, a sample is taken and diluted with water to make an 18 kg dilute sample with of concentration 15 ppm. This diluted sample is then pressurized in the pressure vessel, and the molecular weights of each sample are compared to the 15 ppm General Average line.

### 4.3 Results

A PEO solution with a concentration of 1000 ppm was plunged through the syringe pump at frequencies of 2000, 3600, 8000, and 9300 Hz. *Table 13* below summarizes the results of testing.

*Table 13: Molecular weight results for case study samples.*

Frequency [Hz]	Mass Flow Rate [kg/s]	$M_w * 10^6$ [g/mol]	Error [%]
<b>2000</b>	2.82E-02	3.71	7.25
<b>3600</b>	5.07E-02	3.92	2.05
<b>8000</b>	1.13E-01	6.11	52.65
<b>9300</b>	1.31E-01	29.38	634.50

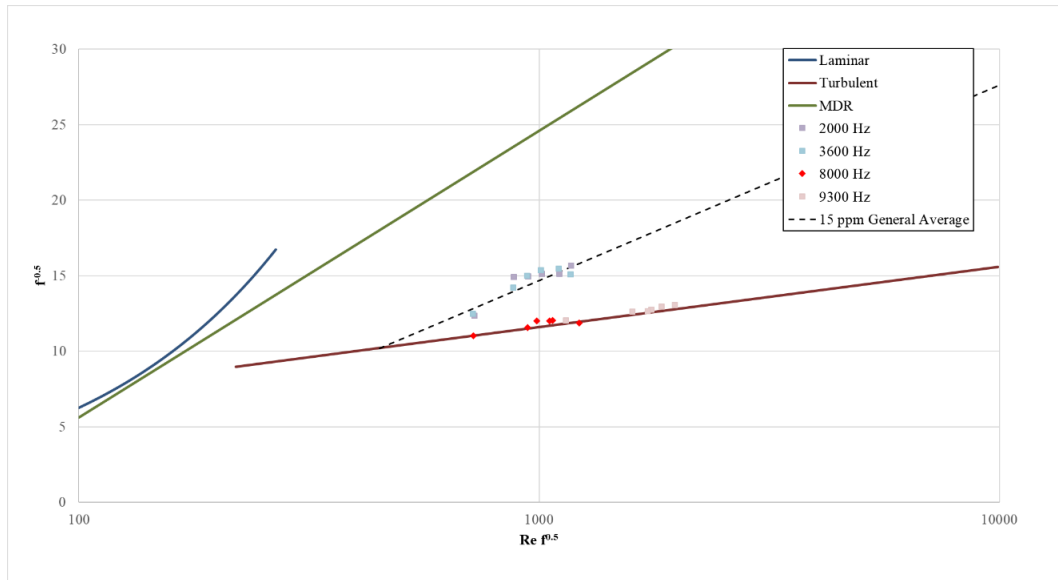


*Figure 23: Demonstration of degradation of polymer solution after being plunged through the syringe pump.*

Looking at Figure 23 and Table 13, it is clear that the samples plunged at higher mass flow rates have degraded. The lower flow rates showed little degradation, reasonably within error. However, there are some concerns regarding the syringe pump that likely affected these results:

- (1) The crossbar of the syringe pump that the leadscrew of the motor attaches to in order to depress the pistons is not completely straight. It is unclear if this is a misalignment due to the position of the parts within the build or if there is an unknown source causing this, but it is very apparent when all 4 pistons are plunged. The two outer pistons clearly do not plunge to the same depth. The difference in plunge depth between the two side pistons is about  $\frac{1}{4}$  “.
- (2) While the system has been calibrated for frequency vs mass flow rate, these are only average values. It was observed many times throughout testing that as the system plunges from start to finish, approximately halfway through a test, the speed of the pistons will slow down slightly, only to resume to the original speed about  $\frac{3}{4}$  into a

single plunge. Furthermore, at this same halfway point, at certain frequencies, the entire platform and syringe pump will begin emitting a mid to high pitched squealing noise, which promptly stops at the same  $\frac{3}{4}$  plunge point. What exactly causes this is unclear, but given this phenomenon becomes more intense (at some points, bolts that were tightened with a wrench were vibrating enough to loosen themselves), it may have something to do with the harmonic frequency of the overall system.

- (3) The syringes are not perfectly sealed. During prolonged, repeated testing, water and polymer solution was seen on the opposite side of 2 of the pistons, where it should be dry. Again, this could be due to the observed misalignment, but the presence of liquid on this side of the pistons did not seem to affect the ability to perform tests.

## CHAPTER V

### SUMMARY AND CONCLUSIONS

The focus of the current work was the establishing of polymer preparation procedures for PEO solutions as well as the methods to characterization the samples. Through repeated preparation and characterization of batches there were three primary conclusions from this work:

- 1) A robust means of characterizing polyethylene oxide solutions was demonstrated. The focus of the characterization was primarily placed on estimating the mean molecular weight and the shear thinning viscosity properties.
- 2) Characterization of prepared batches combined with comparisons with historical data, validated the final polymer preparation procedures. One of the key secondary observations from the development of preparation procedures was that it is critical that prolonged exposure to some metals can significantly accelerate the degradation rate.
- 3) The molecular weight characterization was used to show that a syringe pump designed by Bonk et al. (2017) completely degrades PEO WSR-301 at flow rates of 0.11 kg/s to the point that results were consistent with water, effectively having no drag reduction properties.

## REFERENCES

- Afifi-Effat, A. M. & Hay, J. N. (1971) "The Thermal Stabilization of Polyethylene Oxide." *European Polymer Journal*, 8(2), 289-297.
- Bailey, F.E., & Callard, R.W. (1959). Some Properties of Poly(ethylene oxide) in Aqueous Solution. *Journal of Applied Polymer Science*, 1(1), 56-62.
- Bonk, S., Alec Barker, Melissa Duncan & Erin Peterson (2017) "Low volumetric flow rate injection system," *MAE 4344 Capstone Design Project*, MAE, OSU.
- Elbing, B.R. (2009) "Skin-friction drag reduction within turbulent flows," Ph.D. dissertation, University of Michigan, Ann Arbor.
- Elbing, B.R., Winkel, E.S., Solomon, M.J. & Ceccio, S.L. (2009) "Degradation of homogeneous polymer solutions in high shear turbulent pipe flow," *Experiments in Fluids*, 47, 1033-1044 (doi: 10.1007/s00348-009-0693-7).

- Elbing, B.R., Dowling, D.R., Perlin, M. & Ceccio, S.L. (2010a) “Diffusion of drag-reducing polymer solutions within a rough-walled turbulent boundary layer,” *Physics of Fluids*, 22(4), 045102 (doi: 10.1063/1.3371957).
- Elbing, B.R., Winkel, E.S., Ceccio, S.L., Perlin, M. & Dowling, D.R. (2010b) “High-Reynolds-number turbulent-boundary-layer wall-pressure fluctuations with dilute polymer solutions,” *Physics of Fluids*, 22(8), 085104 (doi:10.1063/1.3478982).
- Elbing, B.R., Solomon, M.J., Perlin, M., Dowling, D.R. & Ceccio, S.L. (2011) “Flow-induced degradation of drag-reducing polymer solutions within a high-Reynolds number turbulent boundary layer,” *Journal of Fluid Mechanics*, 670, 337-364 (doi:10.1017/S0022112010005331).
- Elbing, B.R., Perlin, M., Dowling, D.R. & Ceccio, S.L. (2013) “Modification of the mean near-wall velocity profile of a high-Reynolds number turbulent boundary layer with the injection of drag-reducing polymer solutions,” *Physics of Fluids*, 25(8), 085103 (doi:10.1063/1.4817073).
- Fontaine, A.A., Petrie, H.L., & Brungart, T.A. (1992) “Velocity profile statistics in a turbulent boundary layer with slot-injected polymer,” *Journal of Fluid Mechanics*, 238, 435-466.
- Grandbois, M., Beyer, M., Rief, M. Clausen-Schaumann, H. & Gaub, H.E. (1999) “How strong is a covalent bond,” *Science*, 283(5408), 1727-1730.
- Han, W. J., Dong, Y. Z. & Choi, H. J. (2017) “Applications of water-soluble polymers in turbulent drag reduction,” *Processes*, 5(2), 24.
- Harvey, D. (2016) *Propogation of Uncertainty*. Available at:  
[https://chem.libretexts.org/Textbook\\_Maps/Analytical\\_Chemistry\\_Textbook\\_Maps/Map](https://chem.libretexts.org/Textbook_Maps/Analytical_Chemistry_Textbook_Maps/Map)

%3A\_Analytical\_Chemistry\_2.0\_(Harvey)/04\_Evaluating\_Analytical\_Data/4.3%3A\_Pro  
pagation\_of\_Uncertainty\_[Online: accessed 18 February 2018].

- Hershey, H.C. & Zakin, J.L. (1969a) "Existence of 2 types of drag reduction in pipe flow of dilute polymer solutions," *Industrial & Engineering Chemistry Fundamentals*, 6(3), 381.
- Hershey, H.C. & Zakin, J.L. (1969b) "A molecular approach to predicting onset of drag reduction in turbulent flow of dilute polymer solutions," *Chemical Engineering Science*, 22(12), 1847.
- Hou, Y.X., Somandepalli, V.S.R. & Mungal, M.G. (2008) "Streamwise development of turbulent boundary layer drag reduction with polymer injection," *Journal of Fluid Mechanics* 597, 31-66.
- Kalashnikov, V. N. (1994). Shear-rate dependent viscosity of dilute polymer solutions. *Journal of Rheology*, 38(5), 1385-1403.
- Kalashnikov, V. (1998) "Dynamical Similarity and Dimensionless Relations for Turbulent Drag Reduction by Polymer Additives," *Journal of Non-Newtonian Fluid Mechanics*, 75, 209-230.
- Larson, R.G. (1992) "Instabilities in viscoelastic flows," *Rheologica Acta*, 31(3), 2123-263.
- Larson, R. G. (1999) *The Structure and Rheology of Complex Fluids*. Oxford, New York: Oxford University Press.
- Layec, Y. & Layec-Raphalen, M. N. (1983) "Instability of Dilute Poly(Ethylene-Oxide) Solutions," *Journal de Physique Lettres*, 44(3), pp. 121-128.
- Liaw, G.C., Zakin, J.L. & Patterson, G.K. (1971) "Effect of molecular characteristics of polymers on drag reduction," *AIChE Journal*, 17(2), 391.

- McGary JR, C. W. (1960) "Degradation of Poly(ethylene Oxide)," *Journal of Polymer Science*, 46(147), 51-57.
- McKinley, G. H. (2005). Dimensionless groups for understanding free surface flows of complex fluids. *SOR Rheology Bulletin*, 72(2), 6,8-9,19.
- Mysels, K. J. (1949) "Flow of Thickened Fluids," U.S. Patent 2,492,173, Dec. 27, 1949.
- Omega Engineering (1999) "User's Guide: MODEL PX2300 differential pressure transmitters," SS2043, <https://www.omega.com/manuals/manualpdf/M3244.pdf> (02/26/99 Rev.A).
- Patterson, G.K., Zakin, J.L. & Rodriguez, J.M. (1969) "Drag reduction – polymer solutions soap solutions and solid particle suspensions in pipe flow," *Industrial and Engineering Chemistry*, 61(1), 22.
- Petrie, H.L., Deutsch, S., Brungart, T.A. & Fontaine, A.A. (2003) "Polymer drag reduction with surface roughness in flat-plate turbulent boundary layer flow," *Experiments in Fluids*, 35, 8-23.
- Petrie, H., Fontaine, A.A., Moeny, M & Deutsch, S. (2005) "Experimental study of slot-injected polymer drag reduction," in *Proceedings of the 2<sup>nd</sup> International Symposium on Seawater Drag Reduction*, Busan, Korea, 605-620.
- Shetty, A.M. & Solomon, M.J. (2009) "Aggregation in dilute solutions of high molar mass poly(ethylene) oxide and its effect on polymer turbulent drag reduction," *Polymer*, 50, 261-270.
- Slattery, J. C. (1968) "Dimensional considerations in viscoelastic flows," *AIChE Journal*, 14, 516-518.

- Somandepalli, V.S.R., Hou, Y.X. & Mungal, M.G. (2010) "Concentration flux measurements in a polymer drag-reduced turbulent boundary layer," *Journal of Fluid Mechanics*, 644, 281-319.
- TA Instruments-Waters LLC, 2013. *Introductory Guide to Using a DHR Rheometer*, New Castle, DE: s.n.
- Toms, B.A. (1948) "Some observations on the flow of linear polymer solutions through straight tubes at large Reynolds numbers," *Proceedings of the First International Congress on Rheology*, 2, 135-141.
- Truong, V. (2001). *Drag Reduction Technologies*. Fishermans bend, Victoria, Australia: DSTO Aeronautical and Maritime Research Laboratory. Retrieved from <http://dspace.dsto.defence.gov.au/dspace/handle/1947/3846>
- Vanapalli, S.A., Ceccio, S.L. & Solomon, M.J. (2006) "Universal scaling for polymer chain scission in turbulence," *Proceedings of the National Academy of Sciences of the United States of America*, 103(45), 16660-16665.
- Vanapalli, S.A., Islam, M.T. & Solomon, M.J. (2005) "Scission-induced bounds on maximum polymer drag reduction in turbulent flow," *Physics of Fluids*, **17**(9), 095108.
- Virk P.S. (1975) "Drag reduction fundamentals," *AIChE Journal*, 21 (4), 625-656.
- Virk, P.S., Merrill, E.W., Mickley, H.S., Smith, K.A. & Mollo-Christensen, E.L. (1967) "The Toms phenomenon: turbulent pipe flow of dilute polymer solutions," *Journal of Fluid Mechanics*, 20(2), 305-328.
- Virk, P.S., Mickley, H.S. & Smith, K.A. (1970) "The ultimate asymptote and mean flow structure in Toms' Phenomenon," *Journal of Applied Mechanics*, 37(2), 488-493.

- Wei, T. & Willmarth, W.W. (1992) "Modifying turbulent structure with drag-reducing polymer additives in turbulent channel flows," *Journal of Fluid Mechanics*, 245, 619-641.
- White, C.M., Somandepalli, V.S.R. & Mungal, M.G. (2004) "The turbulence structure of drag-reduced boundary layer flow," *Experiments in Fluids*, 36, 62-69.
- Winkel, E. S., Oweis, G. F., Vanapalli, S. A., Dowling, D. R., Perlin, M., Solomon, M. J., & Ceccio, S. L. (2009) "High-Reynolds-number turbulent boundary layer friction drag reduction from wall-injected polymer solutions," *Journal of Fluid Mechanics*, 621, 259-288.
- Zadrazil, I., Bismarck, A., Hewitt, G.F. & Markides, C.N. (2012) "Shear layers in the turbulent pipe flow of drag reducing polymer solutions," *Chemical Engineering Science*, 72, 142-154.
- Zakin, J.L. & Hunston, D.L. (1980) "Effect of polymer molecular-variables on drag reduction," *Journal of Macromolecular Science-Physics*, B18(5), 795-814.

## APPENDICES

### APPENDIX A: DETAILED POLYMER PREPARATION PROCEDURES

To begin preparing the master solution, first, thoroughly wash and completely dry all storage containers. This will limit any undesired contaminants being unknowingly introduced into the batch during preparation. Next, the desired amount of PEO is measured into a beaker (6 g of PEO for the 15 kg batch of 400 ppm). For the current study, the polymer was measured on a 150-gram digital scale (ED-150 Symmetry, Cole-Parmer, Vernon Hills, IL, USA), which has an accuracy of 0.02 grams. When spooning the polymer, it had a tendency to make puffs and not all end up in the 100 mL glass beaker (Karter Scientific Labware Manufacturing, Lake Charles, LA, USA). When this happened, any excess polymer was blown (gently to prevent scattering PEO around the laboratory) or brushed from the scale to promote an accurate measurement of the sample. Once the desired amount was collected, a pinch (approximately  $\frac{1}{4}$  to  $\frac{1}{2}$  gram) of sodium thiosulfate ( $\text{Na}_2\text{S}_2\text{O}_3$ ), hereafter referred to as STS (217263, Sigma-Aldrich, Darmstadt, Germany), would be added to the beaker and gently mixed in with the PEO using a wooden stirrer. [Note that the STS could also be added directly to the bucket before or after mixing the solution.] The STS is used to neutralize any chlorine that might be in the water supply, as chlorine can rapidly degrade PEO when in solution with water. STS residue and the products of

its reaction with chlorine have been shown to have a negligible impact on polymer drag reduction (Petrie et al., 2003; Elbing et al., 2011). The exact quantity of STS required to completely neutralize all chlorine is unknown since it is dependent on the chlorine level on the given day, but it is expected to be a small amount based on previous reports (Elbing et al., 2011). Best practice is to measure the chlorine level before preparation to estimate the required amount of STS, and then after adding the STS confirm the chlorine level is  $< 0.01$  ppm. The laboratory has a chlorine meter (CL200 ExStik, Extech; CL204 Reagent tablets, Extech), but given the relatively small quantities for the master solution and the low level of chlorine measured it was not used in the current work.

Afterwards, the beaker was taken over to the mixing container (5-gallon bucket), being careful that all the polymer powder remained in the beaker (the smaller particles have a tendency to puff and loft into the air if moved to vigorously). The empty mixing container would be placed on a 35-kg digital bench/floor industrial scale (CPWplus-35, Adam Equipment Inc, Oxford, CT, USA), which has a resolution of 0.01 kg. The scale would be zeroed out (tared) to negate the weight of the bucket, though it should be noted that the 35-kg limit includes the bucket weight. The bucket is then filled with 10% to 20% of the total water to be added (e.g. 2.5 kg of the 15 kg batches). The purpose for this is twofold; (1) it helps reduce misting created by the water jet used to hydrate the polymer that will be discussed subsequently, and (2) it minimizes the amount of polymer added to the bucket that clings to the walls or base of the bucket, which can lead to an uneven distribution of polymer.

Once the bucket has the initial 10-20% of the total water (e.g. 2.5 kg of the 15 kg batches), the beaker containing the mixture of STS and PEO is gently sprinkled into a fanned out water jet, using a gentle shaking action, about 4 to 5 inches above the jet of water. The jet of water was formed with a PVDF plastic flat spray nozzle (Type 632.566, Lechler GmbH; part# 34845K41, McMaster-Carr) that had an  $90^\circ$  spray angle. The flat spray nozzle had a  $\frac{1}{4}$  NPT male inlet that was mounted in a pipe adapter to be connected to a common garden hose fitting ( $\frac{3}{4}$ "

GHT (Garden Hose Thread) or NH (National Hose)). The nozzle fanned the stream of water exiting the hose into a flat, triangular jet. This flat jet helps prevent the formation of polymer aggregates in the water by allowing polymer powder particles to individually contact the water surface, which promotes homogeneous mixing of the polymer solution. It is important that no aggregates exist in the final master solution, as this will lead to a heterogeneous polymer solution, which ultimately results in inconsistent child solutions that are prepared by diluting the master solution.

When filling the bucket with water, the jet attachment will yield a blowback mist, as mentioned above, inside the bucket that can rise out of the bucket. This mist makes it difficult to sprinkle the polymer powder into the jet because it lightly hydrates any polymer powder on the surface inside the beaker causing it to clump. Thus, when mixing, the flow rate needs to be adjusted such that there is sufficient flow rate to form the fanned out jet, while minimizing the mist caused by the blowback.

As the PEO/STS solute is added, between shakes, the fan was gently moved back and forth across the surface of the water to enhance mixing and on the bucket wall to rinse any PEO/STS clinging to the walls. Through trial and error, a nominal mixing rate for the 15 kg batches was 0.6 g of PEO (or about 1/10<sup>th</sup> the contents of the beaker) for every 1 kg of water as displayed on the digital scale appeared to produce the least amount of aggregates. At this rate, the beaker of PEO is empty when 12.5 kg of water has been added. The additional 2.5 kg of water to be added at the end is beneficial for rinsing the beaker and bucket sidewalls. As mentioned above, the mist blowback cannot be completely prevented and consequently there will be some polymer that has hydrated on the inside wall of the beaker. Using the jet, the inside of the beaker was washed out until it was clean of all solutes, allowing them to drain into the bucket. Once the beaker was empty and cleaned out, the addition of water continued while rinsing off any polymer agglomerations that formed on the sidewalls until the scale read 15 kg. The water flow was then

shut off, which it took approximately 10 minutes to fill the 15 kg bucket. Once the mixing is complete, the polymer/water solution must be left to set, allowing the polymer solution to fully hydrate. The bucket was covered and sealed, and the solution was allowed to hydrate for approximately 12-16 hours before use.

## APPENDICES

### APPENDIX B: ANALYSIS CODE

The following is all of the VBA code and file names used to run the analysis program based on the process described in Section 3.1.3. The UserForm1 file also has an image of the GUI layout.

File Name: ThisWorkbook.cls

```
Private Sub Workbook_Open()  
    MsgBox "This software incorporates multiple documents written  
    by Yasaman Farsiani and Marcus Lander, " & _  
    "under the supervision of Dr. Brian Elbing at Oklahoma State  
    University."  
    & vbNewLine & vbNewLine & vbNewLine & _  
    "Virk Tube Visual Data Analysis Tool (Version 1.0.0)" &  
    vbNewLine & _  
    Chr(169) & " 2018 Dr. Brian Elbing, Yasaman Farsiani, and  
    Marcus Lander", , "Notice of Copyright"  
  
End Sub
```

File Name: UserForm1.frm

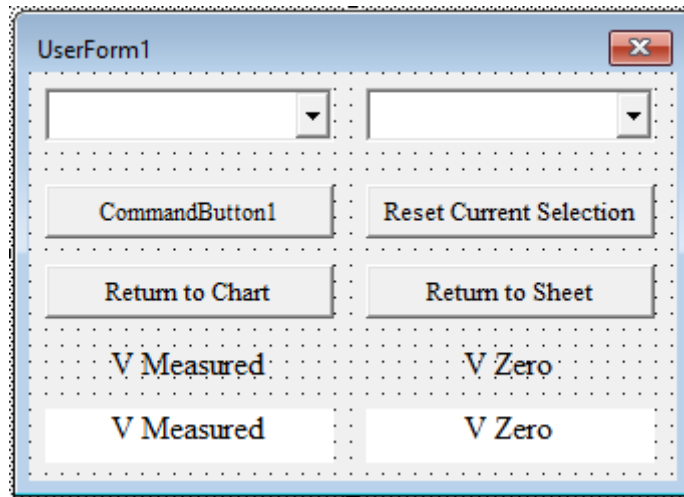


Figure 24: VBA GUI Interface for the visual data analysis program.

```
Public NVS As IndexStorage  
Public ChartObj As Chart  
Dim indecies As Byte  
Dim clsEventChart As New CEventChart  
  
Private Sub ChartCmd_Click()  
    ChartObj.Activate  
End Sub  
  
Private Sub LowerUpperCmbBox_Change()  
    ChartObj.Activate  
  
    With LowerUpperCmbBox  
        ChartObj.Axes(xlCategory).MinimumScale =  
        NVS.Lower(.ListIndex + 1)  
        ChartObj.Axes(xlCategory).MaximumScale =  
        NVS.Upper(.ListIndex + 1)  
        UpdateLabels (.ListIndex + 1)  
    End With  
End Sub
```

```

Private Sub OperationCmbBox_Change()
    If OperationCmbBox.ListIndex = 0 Then
        OperationCmdBtn.Caption = "Submit V Zero data"
    ElseIf OperationCmbBox.ListIndex = 1 Then
        OperationCmdBtn.Caption = "Submit V Measure data"
    End If
End Sub

Private Sub OperationCmdBtn_Click()
    'write values to Sheet1
    Dim i As Long

    Sheet1.Activate

    If OperationCmbBox.ListIndex = 0 Then
        For i = 1 To indecies
            Sheet1.Cells(1 + i, 11).Value = _
                Excel.WorksheetFunction.Average( _
                    Range(Cells(NVS.Vzero(i, 1), 2), Cells(NVS.Vzero(i,
2), 2)))
        Next i
    ElseIf OperationCmbBox.ListIndex = 1 Then
        For i = 1 To indecies
            Sheet1.Cells(1 + i, 10).Value = _
                Excel.WorksheetFunction.Average( _
                    Range(Cells(NVS.Vmeas(i, 1), 2), Cells(NVS.Vmeas(i,
2), 2)))
        Next i
    End If
End Sub

Private Sub ResetCmd_Click()
    NVS.ResetRange OperationCmbBox.ListIndex,
LowerUpperCmbBox.ListIndex + 1
    UpdateLabels (LowerUpperCmbBox.ListIndex + 1)
End Sub

Private Sub SheetCmd_Click()
    Sheet1.Activate
End Sub

Private Sub UserForm_Initialize()
    Dim entry As String, response As String
    Dim i As Long, j As Byte

    Dim xRng As Range, yRng As Range

    entry = 0
    indecies = 0

    If Charts.count = 0 Then End

    Set ChartObj = Charts(1)

    Set clsEventChart.EvtChart = ChartObj

    With OperationCmbBox

```

```

        .AddItem "Range of V Zero", 0
        .AddItem "Range of V Measure", 1
        .ListIndex = 0
End With

ChartObj.Activate

DoEvents

Do Until entry = ""
    indecies = indecies + 1
    entry = Sheet1.Cells(indecies + 2, 5).Value
Loop

Set NVS = New IndexStorage
NVS.InitializeWithValues (indecies)

With LowerUpperCmbBox
    For i = 1 To indecies
        .AddItem CStr(NVS.Lower(i)) + "->" +
CStr(NVS.Upper(i)), i - 1
    Next i

    UpdateLabels 1

    .ListIndex = 0
End With
End Sub

Friend Sub UpdateLabels(ByVal Value As Long)
    With NVS
        VmeasLbl = CStr(.Vmeas(Value, 1)) + "->" +
CStr(.Vmeas(Value, 2))
        VzzeroLbl = CStr(.Vzero(Value, 1)) + "->" +
CStr(.Vzero(Value, 2))
    End With
End Sub

```

---

File Name: Module1.bas

```

Sub Phasel ()

    Dim n As Byte, count As Long, answer As String

    'import new data
    importWorkbook

    count = 0

    'how many data points are there?
    answer = InputBox("How many points?", "Number of Points")

    Select Case answer
        Case ""
            If case1 = "" Then Exit Sub
        Case Else
    
```

```

        n = CByte(answer)
    End Select

    buildTable n

    'Auto Fill
    countContents count, 1, 2, Sheet1
    AutoFillSteps count + 1

    'let the OS take care of some things and catch up
    DoEvents

    'create chart and input data
    MoveChart count + 1

    Sheet1.Activate

    Sheet1.Cells(2, 4).Select

End Sub

Private Sub importWorkbook()

    Dim importWorkbook As Workbook
    Dim importSheet As Worksheet
    Dim homeWorkbook As Workbook
    Dim homeSheet As Worksheet

    Dim filename As String
    Dim filter As String

    Dim count As Long

    Dim importRange As Range

    Set homeWorkbook = ThisWorkbook
    Set homeSheet = homeWorkbook.Sheets(1)

    filter = "Excel Workbooks (*.xlsx),*.xlsx, Excel Macro
Workbooks (*.xslm),*.xslm"

    filename = Application.GetOpenFilename(filter, , "Please
select an input file")

    If filename = "False" Then End

    Set importWorkbook = Application.Workbooks.Open(filename)
    Set importSheet = importWorkbook.Sheets(1)

    countContents count, 1, 2, importSheet

    Set importRange = Range(Cells(1, 1), Cells(count + 1, 2))

    homeSheet.Range(importRange.Address) =
importSheet.Range(importRange.Address).Value

    importWorkbook.Close

```

```

End Sub

Private Sub buildTable(ByRef n As Byte)

    Dim i As Byte
    Dim table As Range

    Set table = Range(Cells(1, 5), Cells(1 + n, 11))

    table(1, 1) = "Lower"
    table(2, 1) = "0"
    table(1, 2) = "Upper"
    table(1, 3) = "Count"
    table(1, 4) = "Mass [kg]"
    table(1, 5) = "Time [s]"
    table(1, 6) = "Vmeas [V]"
    table(1, 7) = "Vzero [V]"
    table(1, 8) = "Temp [F]"

    'update if needed
    DoEvents

    For i = 1 To n
        table(i + 1, 3) = i
    Next i

    'Add in backwards referencing
    AutoFillRange 3, 1 + n, 5, 5, Sheet1, "=R[-1]C[1]"

    'update if needed
    DoEvents

End Sub

Private Sub AutoFillRange(ByVal row1 As Long, ByVal row2 As Long,
ByVal column1 As Long, ByVal column2 As Long, ByRef Sheet As
Worksheet, ByVal Formula As String)

    With Sheet
        .Activate
        .Cells(row1, column1).FormulaR1C1 = Formula
        .Cells(row1, column1).autofill
    Destination:=Range(.Cells(row1, column1), .Cells(row2, column2))
    End With
End Sub

Private Sub MoveChart(ByVal count As Long)

    Dim ThisChart As Chart
    Set ThisChart = Charts.Add

    With ThisChart
        .ChartType = xlXYScatter
        .SeriesCollection.NewSeries
        .FullSeriesCollection(1).XValues = CStr("='Quick
Analysis'!R2C3:R" + CStr(count) + "C3")
    End With
End Sub

```

```

        .FullSeriesCollection(1).Values = CStr("'Quick
Analysis'!R2C2:R" + CStr(count) + "C2")
    End With

End Sub

Private Sub AutoFillSteps(ByVal count As Long)

    With Sheet1
        .Cells(1, 3).Value = "Step"
        .Cells(2, 3).Value = 2
        .Cells(3, 3).Value = 3

        Range(.Cells(2, 3), .Cells(3, 3)).autofill
        Destination:=Range(.Cells(2, 3), .Cells(count, 3))

        'move to an arbitrarily unused cell. DO NOT DELETE THIS OR
        THE CHART BREAKS
        Cells(2, 19).Select
    End With

End Sub

Private Sub countContents(ByRef Value As Long, ByVal rowStart As
Long, ByVal col As Long, Sheet As Worksheet)

    Do Until Sheet.Cells(rowStart + Value, col).Value = ""
        Value = Value + 1
    Loop

    Value = Value - 1
End Sub

Sub Phase2()
    UserForm1.Show vbModeless
End Sub

```

---

File Name: CEventChart.cls

```

Public WithEvents EvtChart As Chart

Private Sub EvtChart_Select(ByVal ElementID As Long, ByVal Arg1
As Long, ByVal Arg2 As Long)
    Dim frm As Object
    Dim formCount As Byte

    For Each frm In UserForms
        formCount = formCount + 1
    Next frm

    If formCount = 0 Then Exit Sub

    Dim OpBox As ComboBox
        Set OpBox = UserForm1.OperationCmbBox

    Dim RangeBox As ComboBox

```

```

        Set RangeBox = UserForm1.LowerUpperCmbBox

    If Arg2 > 0 Then
        x = ActiveChart.SeriesCollection(Arg1).XValues
        For i = LBound(x) To UBound(x)
            If i = Arg2 Then
                With UserForm1.NVS

                    If OpBox.ListIndex = 0 Then
                        If .Vzero(RangeBox.ListIndex + 1, 1) = 0
                            Then
                                .Vzero(RangeBox.ListIndex + 1, 1) =
                                x(i)
                            ElseIf x(i) < .Vzero(RangeBox.ListIndex +
                                1, 1) Then
                                .Vzero(RangeBox.ListIndex + 1, 1) =
                                x(i)
                            ElseIf .Vzero(RangeBox.ListIndex + 1, 1)
                                <> 0 Then
                                .Vzero(RangeBox.ListIndex + 1, 2) =
                                x(i)
                            End If

                        ElseIf OpBox.ListIndex = 1 Then
                            If .Vmeas(RangeBox.ListIndex + 1, 1) = 0
                                Then
                                    .Vmeas(RangeBox.ListIndex + 1, 1) =
                                    x(i)
                                ElseIf x(i) < .Vmeas(RangeBox.ListIndex +
                                    1, 1) Then
                                    .Vmeas(RangeBox.ListIndex + 1, 1) =
                                    x(i)
                                ElseIf .Vmeas(RangeBox.ListIndex + 1, 1)
                                    <> 0 Then
                                    .Vmeas(RangeBox.ListIndex + 1, 2) =
                                    x(i)
                                End If
                            End If

                        UserForm1.UpdateLabels (RangeBox.ListIndex +
                        1)

                    End With
                Exit For
            End If
        Next i
    End If
End Sub

```

---

File Name: IndexStorage.cls

```

' Properties
Private pLower() As Long
Private pUpper() As Long

Private pVmeas() As Double
Private pVzero() As Double

```

```

'Methods
Public Property Get Lower(index As Long) As Long
    Lower = pLower(index)
End Property

Public Property Let Lower(index As Long, Value As Long)
    pLower(index) = Value
End Property

Public Property Get Upper(index As Long) As Long
    Upper = pUpper(index)
End Property

Public Property Let Upper(index As Long, Value As Long)
    pUpper(index) = Value
End Property

Public Property Get Vmeas(index1 As Long, index2 As Long) As Long
    Vmeas = pVmeas(index1, index2)
End Property

Public Property Let Vmeas(index1 As Long, index2 As Long, Value
As Long)
    pVmeas(index1, index2) = Value
End Property

Public Property Get Vzero(index1 As Long, index2 As Long) As Long
    Vzero = pVzero(index1, index2)
End Property

Public Property Let Vzero(index1 As Long, index2 As Long, Value
As Long)
    pVzero(index1, index2) = Value
End Property

Private Sub Class_Initialize()
End Sub

Friend Sub InitializeWithValues(ByVal n As Long)

    Dim i As Long

    ReDim pVmeas(1 To n, 1 To 2)
    ReDim pVzero(1 To n, 1 To 2)

    ReDim pLower(1 To n)
    ReDim pUpper(1 To n)

    For i = 1 To n
        Lower(i) = Sheet1.Cells(i + 1, 5)
        Upper(i) = Sheet1.Cells(i + 1, 6)
    
```

```
Next i

End Sub

Friend Sub ResetRange (ByVal OpIndex As Long, RangeIndex As Long)

    If OpIndex = 0 Then
        Vzero (RangeIndex, 1) = 0
        Vzero (RangeIndex, 2) = 0
    ElseIf OpIndex = 1 Then
        Vmeas (RangeIndex, 1) = 0
        Vmeas (RangeIndex, 2) = 0
    End If

End Sub
```

## APPENDICES

### APPENDIX C: EXTENDED UNCERTAINTY ANALYSIS DATA

The following is an extended set of data calculated in the molecular weight uncertainty analysis such that the variables presented herein are directly dependent upon the independent variables of the entire system, per data point.

Table 14: Extended uncertainty data for concentration 15 ppm.

Uncertainty 15 ppm											
$\Delta p$ (Pa)	$\epsilon_{\Delta p}$	U (m/s)	$\epsilon_U$	Re	$\epsilon_{Re}$	f	$\epsilon_f$	Re f <sup>0.5</sup>	$\epsilon_{Re f^{0.5}}$	f <sup>-0.5</sup>	$\epsilon_{f^{-0.5}}$
456.61	344.59	0.56	1.69E-02	6.5E+03	196	7.4E-03	5.65E-03	561	214.02	11.6	-4.42
740.45	344.66	0.79	1.86E-02	9.1E+03	214	6.2E-03	2.93E-03	714	170.08	12.7	-3.02
979.44	344.69	0.96	1.94E-02	1.1E+04	224	5.5E-03	2.00E-03	821	149.71	13.4	-2.44
793.38	344.67	0.82	1.85E-02	9.4E+03	214	6.1E-03	2.72E-03	739	164.72	12.8	-2.83
489.81	344.57	0.58	1.56E-02	6.7E+03	180	7.4E-03	5.28E-03	581	206.66	11.6	-4.11
626.48	344.45	0.69	9.77E-03	8.0E+03	113	6.8E-03	3.79E-03	657	182.78	12.1	-3.36
1123.26	344.73	1.05	2.06E-02	1.2E+04	237	5.2E-03	1.66E-03	876	140.56	13.8	-2.20
511.68	344.61	0.61	1.73E-02	7.0E+03	199	7.2E-03	4.86E-03	591	201.77	11.8	-4.02
708.34	344.64	0.77	1.80E-02	8.9E+03	208	6.2E-03	3.05E-03	696	172.83	12.7	-3.15
439.57	344.58	0.54	1.64E-02	6.2E+03	189	7.7E-03	6.12E-03	548	217.09	11.4	-4.49
616.90	344.63	0.70	1.78E-02	8.0E+03	204	6.5E-03	3.70E-03	649	184.49	12.4	-3.50
593.78	344.41	0.66	7.13E-03	7.6E+03	82	7.0E-03	4.08E-03	637	186.55	12.0	-3.50
1218.76	344.77	1.11	2.14E-02	1.3E+04	250	5.1E-03	1.52E-03	924	137.61	13.9	-2.06
1506.84	344.84	1.29	2.38E-02	1.5E+04	277	4.7E-03	1.14E-03	1027	126.66	14.6	-1.78
1052.49	344.74	1.00	2.04E-02	1.2E+04	238	5.4E-03	1.84E-03	858	146.41	13.6	-2.30
744.17	344.66	0.78	1.81E-02	9.1E+03	211	6.3E-03	2.97E-03	722	171.02	12.6	-2.97
489.40	344.61	0.58	1.71E-02	6.7E+03	199	7.6E-03	5.41E-03	585	208.72	11.5	-4.07
346.77	344.56	0.45	1.62E-02	5.3E+03	189	8.7E-03	8.66E-03	493	246.76	10.7	-5.37
638.83	344.62	0.71	1.75E-02	8.3E+03	204	6.5E-03	3.54E-03	669	183.63	12.4	-3.40
1833.89	344.77	1.49	2.29E-02	1.7E+04	266	4.3E-03	8.73E-04	1130	117.14	15.3	-1.57
2095.64	344.86	1.74	2.88E-02	2.0E+04	335	3.6E-03	6.59E-04	1208	113.03	16.7	-1.54
3007.20	345.62	2.13	4.58E-02	2.5E+04	532	3.4E-03	4.92E-04	1447	108.87	17.1	-1.23
5079.80	347.44	2.96	7.77E-02	3.4E+04	904	3.0E-03	3.44E-04	1886	119.04	18.3	-1.05
5174.16	347.90	2.98	8.31E-02	3.5E+04	968	3.0E-03	3.48E-04	1903	122.18	18.2	-1.05
4807.20	346.86	2.82	6.74E-02	3.3E+04	784	3.1E-03	3.60E-04	1835	114.31	17.9	-1.03
4076.45	346.21	2.54	5.62E-02	3.0E+04	653	3.3E-03	3.99E-04	1687	109.60	17.5	-1.07
3174.99	345.59	2.16	4.39E-02	2.5E+04	511	3.5E-03	4.86E-04	1489	107.60	16.9	-1.17
3199.98	347.52	2.20	7.23E-02	2.5E+04	832	3.4E-03	5.06E-04	1481	119.79	17.1	-1.26
2731.67	346.13	2.00	5.32E-02	2.3E+04	612	3.5E-03	5.55E-04	1368	113.38	16.8	-1.32
2382.74	346.12	1.83	5.22E-02	2.1E+04	601	3.7E-03	6.38E-04	1278	116.67	16.5	-1.43
1865.52	345.36	1.55	3.78E-02	1.8E+04	435	4.0E-03	8.25E-04	1131	119.61	15.8	-1.63
1253.83	344.91	1.15	2.58E-02	1.3E+04	297	4.9E-03	1.41E-03	927	135.45	14.3	-2.07
1737.68	345.01	1.43	2.86E-02	1.7E+04	334	4.4E-03	9.45E-04	1103	121.28	15.1	-1.64
867.94	344.67	0.89	1.89E-02	1.0E+04	220	5.7E-03	2.30E-03	780	159.30	13.3	-2.70
2236.19	345.36	1.71	3.73E-02	2.0E+04	435	3.9E-03	6.99E-04	1251	114.33	15.9	-1.41
1368.32	344.88	1.22	2.52E-02	1.4E+04	293	4.7E-03	1.26E-03	979	131.93	14.5	-1.93

Table 15: Extended uncertainty data for concentration 10 ppm.

Uncertainty 10 ppm											
$\Delta p$ (Pa)	$\epsilon_{\Delta p}$	U (m/s)	$\epsilon_U$	Re	$\epsilon_{Re}$	f	$\epsilon_f$	Re f <sup>0.5</sup>	$\epsilon_{Re} \epsilon_f^{0.5}$	f <sup>-0.5</sup>	$\epsilon_f^{0.5}$
4105.33	348.25	2.29	6.73E-02	2.6E+04	775	4.0E-03	5.18E-04	1677	118.18	15.7	-1.01
1608.51	345.17	1.24	2.73E-02	1.4E+04	314	5.4E-03	1.26E-03	1050	123.87	13.6	-1.57
2787.81	346.23	1.76	4.32E-02	2.0E+04	497	4.6E-03	7.11E-04	1382	111.35	14.7	-1.13
2590.99	346.24	1.70	4.35E-02	2.0E+04	501	4.7E-03	7.54E-04	1332	113.20	14.7	-1.19
2948.41	347.04	1.86	5.38E-02	2.1E+04	620	4.4E-03	6.66E-04	1421	115.20	15.1	-1.14
921.49	344.62	0.87	1.60E-02	1.0E+04	184	6.3E-03	2.40E-03	795	152.99	12.6	-2.42
813.82	344.58	0.80	1.47E-02	9.3E+03	170	6.5E-03	2.81E-03	747	161.76	12.4	-2.68
1143.31	344.74	1.02	1.95E-02	1.2E+04	224	5.6E-03	1.77E-03	884	139.44	13.3	-2.08
755.19	344.53	0.77	1.30E-02	8.8E+03	149	6.7E-03	3.08E-03	718	167.00	12.3	-2.84
2893.06	346.00	1.83	4.16E-02	2.1E+04	478	4.5E-03	6.62E-04	1406	109.30	15.0	-1.11
1060.40	344.65	0.94	1.62E-02	1.1E+04	187	6.2E-03	2.09E-03	851	143.56	12.7	-2.13
3696.07	347.58	2.16	6.12E-02	2.5E+04	704	4.1E-03	5.46E-04	1589	115.16	15.6	-1.04
3105.42	346.81	1.92	5.13E-02	2.2E+04	591	4.4E-03	6.34E-04	1457	112.73	15.1	-1.10
1920.45	345.34	1.40	3.09E-02	1.6E+04	355	5.0E-03	1.01E-03	1146	117.31	14.1	-1.41
4605.04	350.36	2.44	8.41E-02	2.8E+04	970	4.0E-03	5.08E-04	1779	128.92	15.8	-1.01
4332.64	348.77	2.35	7.10E-02	2.7E+04	819	4.1E-03	5.13E-04	1725	120.64	15.7	-0.99
2853.19	346.12	1.80	4.23E-02	2.1E+04	488	4.6E-03	6.86E-04	1400	110.46	14.8	-1.12
1451.55	344.90	1.17	2.24E-02	1.3E+04	259	5.5E-03	1.39E-03	999	127.45	13.5	-1.70
1144.65	344.77	1.00	1.97E-02	1.2E+04	229	5.9E-03	1.83E-03	894	141.04	13.1	-2.04
1477.77	344.94	1.19	2.35E-02	1.4E+04	273	5.4E-03	1.35E-03	1016	127.83	13.6	-1.69
442.65	344.42	0.53	8.10E-03	6.2E+03	94	8.0E-03	6.26E-03	556	217.64	11.2	-4.37
3725.83	347.94	2.14	6.29E-02	2.5E+04	731	4.2E-03	5.64E-04	1613	117.93	15.4	-1.03

## APPENDICES

### APPENDIX D: NOMENCLATURE

The following is a list of variables and scripts used in this work, in order of appearance.

### Nomenclature List

Variable	Description
$\%DR$	The total percentage of drag reduction
$\Delta P_s$	Standard pressure drop experienced in a pipe
$\Delta P_p$	Pressure drop in a pipe with in the presence of a drag reducing solution
$n_o$	Number of bonds per monomer
$l_o$	Bond length
$MW, M_w$	Molecular weight
$C$	Concentration of polymer in a solution; in equation <b>3.12</b> is the hypotenuse of a triangle
$m_{polymer}$	Mass of polymer
$m_{solution}$	Mass of solution
$\gamma^*$	Shear rate at the onset of drag reduction
$CV$	Control volume
$M_{sys}$	Mass of a system within a CV
$dA$	Differential area
$u_{out}$	Velocity profile leaving a CV
$u_{in}$	Velocity profile enter a CV
$F_x$	Force in the x-direction
$F_f$	Skin-friction force
$\tau_w$	Wall shear stress
$d$	Inner diameter
$\Delta x$	Length of a CV
$F_{\Delta p}$	Pressure differential force
$p_{in}$	Inlet pressure
$p_{out}$	Outlet pressure
$\rho$	Density
$g$	Acceleration due to gravity
$H, h$	height
$f$	Fanning friction factor ; in equation 4.1, represents frequency
$Re$	Reynolds number
$C_{diluted}$	Diluted concentration
$C_{master}$	Concentration of a Master solution or batch
$m_{master}$	Mass of a Master solution of batch
$m_{add}$	Mass of water added to a solution
$V_{zero}, V_0$	Baseline voltage at a zero-pressure differential
$V_{Measure}$	An elevated voltage level due to a pressure differential
$\bar{V}$	Average voltage over a given range
$A$	Slope of a line ; used as Area in uncertainty analysis
$B$	Y-intercept of a line
$(\_)*$	Denoting that this variable is considered to be measured at the onset of drag reduction
$\nu$	Kinematic viscosity
$U$	Average velocity within a pipe

$\epsilon$	Uncertainty for any variable, according to the subscript
$\sigma$ , Std.Dev	Standard deviation
$d_{watch}$	Resolution of a stopwatch
$t$	Time
$t_{avg}$	Average of time
$t_{target}$	Target time
$a_{hole}$	Hole-center accuracy
$L$	Actual length ; in equation 3.43, represents Length Ratio
$d_{tape}$	Tape measure resolution
$d_{CP}$	Display resolution of the Cole_Parmer scale
$m_{actual}$	Actual mass
$m_{beaker}$	Leftover mass contained in the beaker
$d_{35}$	Display resolution of the CPWplus-35 scale
$m_{bucket}$	Leftover mass contained in a bucket
$d_{PT}$	Resolution of the pressure transducer
$H_2O$	Chemical forumula for water
$r_t$	Radius of a tube
$w$	Distance between two buckets
$r_1$	Radius of bucket 1
$r_2$	Radius of bucket 2
$\dot{m}$	Mass flow rate
$V$	Volume
$z$	Height at a given point
$m_{calibrated}$	Calibration factor for the pressure transducer
$\mu$	Viscosity
$\mu_0$	Zero-shear-rate viscosity
$\mu_\infty$	Infinite-shear-rate viscosity
$\mu_s$	Viscosity of a solvent
$\mu^*$	Viscosity ratio
$\lambda$	Relaxation time
$\lambda_z$	Relaxation time according to Zimm model
$\lambda_k$	Relaxation time according to Kalashnikov model
$[\eta]_0$	Intrinsic viscosity
$C^*$	Overlap concentration
$R$	Ideal gas constant
$T$	Temperature
$T_c$	Temperature in Celsius
$Wi$	Weissenberg number
$\Delta$	When standing alone, represents the difference in limiting viscosities
$L_{ext}$	Length of a fully extended polymer chain
$L_{coil}$	Length of a completely coiled polymer chain
$M_0$	Molar mass

VITA

Marcus David Lander

Candidate for the Degree of

Master of Science

Thesis: PREPARATION AND CHARACTERIZATION OF POLYETHYLENE-  
OXIDE (PEO) SOLUTION

Major Field: Mechanical and Aerospace Engineering

Biographical:

Education:

Completed the requirements for the Master of Science in Mechanical and  
Aerospace Engineering at Oklahoma State University, Stillwater, Oklahoma in  
May, 2018.

Completed the requirements for the Bachelor of Science in Mechanical  
Engineering at Oklahoma State University, Stillwater, Oklahoma in 2015.

Completed the requirements for the Bachelor of Science in Aerospace  
Engineering at Oklahoma State University, Stillwater, Oklahoma in 2015.

Experience:

Graduate researcher in the Experimental Flow Physics Laboratory at Oklahoma  
State University

Professional Memberships:

None currently